

Zoo of axionic wormholes

Caroline Jonas^{1,*}, George Lavrelashvili^{2,†} and Jean-Luc Lehners^{1,‡}¹Max Planck Institute for Gravitational Physics (Albert Einstein Institute), 14476 Potsdam, Germany²Department of Theoretical Physics, A. Razmadze Mathematical Institute at I. Javakhishvili Tbilisi State University, GE-0193 Tbilisi, Georgia

(Received 6 July 2023; accepted 1 September 2023; published 18 September 2023)

As was discovered some time ago by Giddings and Strominger (GS), an axion can support a wormhole geometry in the presence of a massless dilaton, as long as the dilaton coupling remains below a critical value. We find that when the dilaton becomes massive, the set of solutions is vastly increased: not only do solutions exist above the critical value of the coupling, but new branches of solutions with several minima in the geometry also appear. All of these generalized GS-like solutions possess the property that, when analytically continued, they lead to a contracting baby universe. We show that in addition there exist families of solutions which, upon analytic continuation, lead to expanding baby universes. A curious property of axion-dilaton wormhole families is that their Euclidean action often decreases when the solutions acquire additional oscillations in the fields. When we replace the dilaton by an ordinary scalar field with a double well potential, we find analogous wormhole families leading to expanding baby universes. This time the Euclidean action has the expected behavior of increasing with the number of oscillations in the fields, although it also contains a puzzling aspect in that some solutions possess a negative action.

DOI: [10.1103/PhysRevD.108.066012](https://doi.org/10.1103/PhysRevD.108.066012)

I. INTRODUCTION

The questions of the possibility and consequences of topology change have haunted quantum gravity research for several decades now. The simple fact that in a theory of quantum gravity the spacetime manifold should be able to fluctuate suggests that the overall topology of the manifold might also vary and that, on the smallest scales, one might have to think of spacetime as having a foamlike structure [1,2]. With the discovery of explicit wormhole solutions sourced by axions [3], a number of questions became more concrete. For instance, if baby universes can be created locally, then they can carry information away, leading to apparent nonunitary behavior [4–7]. Also, if wormholes can connect distant spatial regions, then their presence will influence the value of coupling constants, effectively leading to random values of said “constants.” Closer inspection of this question led Coleman to the picture of α -vacua, describing superselection sectors of

quantum gravity within which quantum coherence would be individually retained [8].

More recently, these questions have received renewed interest, as it was realized that puzzling features remained: for instance, it is a general expectation that quantum gravity should admit no free parameters [9], and this expectation is in obvious conflict with the above-mentioned α -parameters. Also, in the context of the AdS/CFT correspondence, if there are multiple disconnected boundary regions, then one would expect the CFT partition function to factorise correspondingly. However, if wormholes can connect the asymptotic regions, then they lead to interactions mediated via the bulk—again we encounter a paradox [10–12]. Possible resolutions have been suggested: on the one hand, wormholes might admit negative modes and thus not contribute to the gravitational path integral [13] (though for purely axionic wormholes, the recent work [14] casts doubt on this possibility by showing that these particular wormholes do not admit negative modes). On the other hand, it has been suggested that in the gravitational path integral there might be a huge degeneracy arising from the interplay of states of various topologies [15], perhaps effective enough to reduce the baby universe Hilbert space to a single dimension and obviate the need for α -parameters [16].

These puzzles remain unresolved to date, and motivate us to further study the existence and properties of wormholes (see also [17–23] for related recent works, and [24,25] for useful reviews). A full wormhole solution can be thought

* caroline.jonas@aei.mpg.de

† george.lavrelashvili@tsu.ge

‡ jlehners@aei.mpg.de

Published by the American Physical Society under the terms of the [Creative Commons Attribution 4.0 International license](https://creativecommons.org/licenses/by/4.0/). Further distribution of this work must maintain attribution to the author(s) and the published article's title, journal citation, and DOI. Funded by SCOAP³.

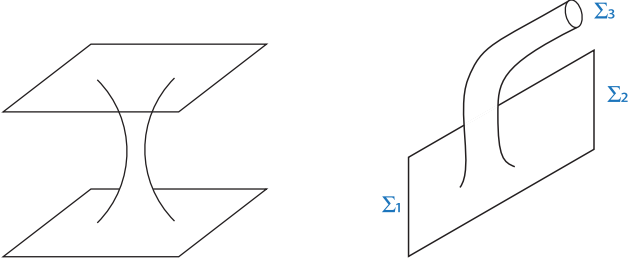


FIG. 1. Common interpretations of Euclidean wormholes. On the left, a full wormhole connecting two asymptotic regions. On the right, a semi-wormhole, leading to the creation of a baby universe (Σ_3).

of [3,17,18] as a (gravitational) instanton-anti-instanton pair connecting two asymptotic regions, whereas a semiwormhole is interpreted as a gravitational instanton mediating a topology change $\Sigma_1 \rightarrow \Sigma_2 \oplus \Sigma_3$, e.g. $\mathbb{R}^3 \rightarrow \mathbb{R}^3 \oplus S^3$, and leading to the creation of a baby universe, see Fig. 1. It was noted in [26] that Giddings-Strominger (GS) wormholes [such as those depicted in Fig. 2(a)] lead to contracting baby universes after analytic continuation to Minkowski time. In contrast, wormholes leading to expanding baby universes should have a wineglass shaped neck, as that depicted in Fig. 2(b). Such wormholes were first found in [26] in a theory of axion-scalar gravity with an asymmetric double well scalar potential, and further elaborated on in [27].

In the present paper we describe many new families of wormhole solutions, both in axion-dilaton gravity with a massive dilaton (greatly extending the results of [22]) and in axion-scalar theory with a symmetric double well potential. We classify the solutions with regard to the distinction mentioned above, namely whether after analytic continuation they lead to contracting baby universes, or to expanding baby universes. Much less is known about the latter class, but even for the former we uncover a surprisingly intricate structure, for a preview see Fig. 9. In all cases we calculate the Euclidean action and find some

unexpected features, which we will describe in detail below. Upon variation of the parameters of the theory and/or the axion charge, the wormhole solutions can develop oscillations both in the scalar/dilaton field and in the scale factor of the universe, see Fig. 2(c). The physical significance of these oscillations remains to be clarified, in particular as it is related to some of the surprising features of the Euclidean action that we find. At critical values of the parameters, entire new families of solutions emerge in bifurcating patterns, a property which for instance implies that these new branches of solutions are not continuously connected to the massless limit of the axion-dilaton theory and thus explains why these wormhole solutions have gone unnoticed so far. Overall, our main realization is that significantly more wormhole solutions exist than hitherto suspected. It is our hope that a better understanding of these concrete wormhole solutions will help in elucidating the conceptual puzzles described above.

II. AXION-DILATON AND AXION-SCALAR GRAVITATIONAL THEORIES

A. Action, field equations, and ansatz

Our starting point is the Euclidean action for gravity coupled to an axion and a dilaton/scalar ϕ , which reads [22]:

$$S_E = \int d^4x \sqrt{g} \left(-\frac{1}{2\kappa} R + \frac{1}{2} \nabla_\mu \phi \nabla^\mu \phi + V(\phi) + \frac{1}{12f^2} e^{-\beta\phi\sqrt{\kappa}} H_{\mu\nu\rho} H^{\mu\nu\rho} \right), \quad (1)$$

where $\kappa \equiv M_{\text{Pl}}^{-2} = 8\pi G$, the dilatonic coupling constant is denoted β and the potential $V(\phi)$, $H_{\mu\nu\rho}$ being the 3-form field strength of an axion field with coupling f . When $\beta \neq 0$, we refer to ϕ as a dilaton, while for $\beta = 0$ we simply call it a scalar. Note that we do not add a Gibbons-Hawking-York boundary term to the action, as we will discuss in more detail below. The corresponding equations of motions are

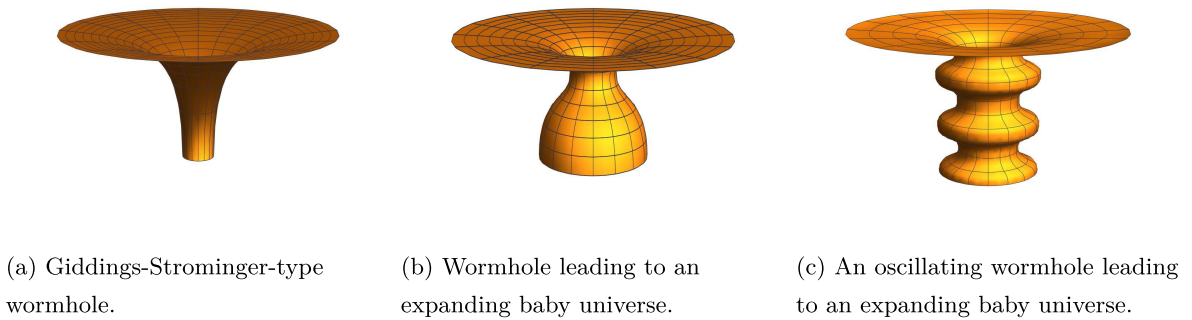


FIG. 2. Visualization of Euclidean wormholes. Wormholes of GS type lead to contracting baby universes upon analytic continuation, while wineglass shaped wormholes lead to expanding baby universes. The right panel shows the oscillating solution with 2 extra minima of the scale factor included in Fig. 27. See Appendix A for further details on embedding diagrams of the sort shown here.

$$\begin{cases} R_{\mu\nu} = \kappa\partial_\mu\phi\partial_\nu\phi + \kappa V g_{\mu\nu} + \frac{\kappa}{2f^2} e^{-\beta\phi\sqrt{\kappa}} H_{\mu\rho\sigma} H_\nu^{\rho\sigma} - \frac{\kappa}{6f^2} e^{-\beta\phi\sqrt{\kappa}} H_{\gamma\rho\sigma} H^{\gamma\rho\sigma} g_{\mu\nu}, \\ \frac{1}{\sqrt{g}} \partial_\mu(\sqrt{g} g^{\mu\nu} \partial_\nu\phi) = \frac{\partial V}{\partial\phi} - \frac{\beta\sqrt{\kappa}}{12f^2} e^{-\beta\phi\sqrt{\kappa}} H_{\gamma\rho\sigma} H^{\gamma\rho\sigma}, \\ \partial_\mu(\sqrt{g} e^{-\beta\phi\sqrt{\kappa}} H^{\mu\rho\sigma}) = 0. \end{cases} \quad (2)$$

We will focus on the following spherically symmetric and homogeneous ansatz

$$\begin{cases} ds^2 = h^2(\tau)d\tau^2 + a(\tau)^2 d\Omega_3^2, \\ \phi = \phi(\tau), \\ H_{0ij} = 0, \quad H_{ijk} = q\epsilon_{ijk}, \end{cases} \quad (3)$$

which leads to the reduced action

$$S_E^{\text{red}} = 2\pi^2 \int d\tau \left(-\frac{3a\dot{a}^2}{\kappa h} + \frac{a^3\dot{\phi}^2}{2h} - \frac{3ah}{\kappa} + ha^3V + \frac{N^2h}{a^3} e^{-\beta\phi\sqrt{\kappa}} \right) + 2\pi^2 \int d\tau \frac{d}{d\tau} \left(\frac{3a^2\dot{a}}{\kappa h} \right), \quad (4)$$

where

$$N^2 \equiv \frac{q^2}{2f^2}, \quad (5)$$

and the overdot denotes a derivative with respect to the (Euclidean) time coordinate τ . Note that the axion charge q is quantized in string theory (when seen as a source for branes, this follows from the associated Dirac quantization condition [28]), and hence q and consequently also N should be thought of as being proportional to integers. The surface term arose from integration by parts, and is important in order to obtain the correct value of the action. Varying the reduced action (4) with respect to a , h , and ϕ yields the following equations of motion [strictly equivalent to (2) in the spherically symmetric ansatz (3)]:

$$\begin{cases} \frac{2a\ddot{a}}{h} + \frac{\dot{a}^2}{h} - h - \frac{2a\dot{a}\dot{h}}{h^2} + \kappa a^2 \left(\frac{\dot{\phi}^2}{2h} + hV(\phi) \right) - \frac{\kappa N^2 h}{a^4} e^{-\beta\phi\sqrt{\kappa}} = 0, \\ \frac{\dot{a}^2}{h^2} - 1 = \frac{\kappa a^2}{3} \left(\frac{\dot{\phi}^2}{2h^2} - V(\phi) \right) - \frac{\kappa N^2}{3a^4} e^{-\beta\phi\sqrt{\kappa}}, \\ \ddot{\phi} + \left(\frac{3\dot{a}}{a} - \frac{\dot{h}}{h} \right) \dot{\phi} = h^2 \frac{dV}{d\phi} - \frac{\beta N^2 h^2 \sqrt{\kappa}}{a^6} e^{-\beta\phi\sqrt{\kappa}}. \end{cases} \quad (6)$$

In the gauge $h \equiv 1$, these equations simplify to

$$\begin{cases} 2a\ddot{a} + \dot{a}^2 - 1 + \kappa a^2 \left(\frac{\dot{\phi}^2}{2} + V(\phi) \right) - \frac{\kappa N^2}{a^4} e^{-\beta\phi\sqrt{\kappa}} = 0, \\ \dot{a}^2 - 1 = \frac{\kappa a^2}{3} \left(\frac{\dot{\phi}^2}{2} - V(\phi) \right) - \frac{\kappa N^2}{3a^4} e^{-\beta\phi\sqrt{\kappa}}, \\ \ddot{\phi} + \frac{3\dot{a}}{a} \dot{\phi} = \frac{dV}{d\phi} - \frac{\beta N^2 \sqrt{\kappa}}{a^6} e^{-\beta\phi\sqrt{\kappa}}. \end{cases} \quad (7)$$

Using the trace of the first equation in (2), the on-shell action of the wormhole solution can be easily calculated

$$S_E = \int d^4x \sqrt{g} \left(\frac{e^{-\beta\phi\sqrt{\kappa}}}{6f^2} H^2 - V(\phi) \right) \quad (8)$$

$$= 2\pi^2 \int d\tau h a^3 \left(\frac{2N^2 e^{-\beta\phi\sqrt{\kappa}}}{a^6} - V(\phi) \right), \quad (9)$$

where in the second line we used the spherically symmetric ansatz. Note that this expression for the on-shell action is equivalent to the action (4) upon using the constraint (6) and keeping the surface term. From this expression of the action (9) we can conclude that for some potentials the wormhole action can become negative.¹ In Sec. IV we will encounter numerical examples confirming this expectation.

The GS wormhole solution [3] has $V = 0$ and in the gauge $a = \tau$ can be written as [17]

$$\begin{aligned} a(\tau) &= \tau, & h(\tau) &= \left(1 - \frac{a_0^4}{\tau^4} \right)^{-1/2}, \\ e^{\beta\phi(\tau)\sqrt{\kappa}} &= \frac{\kappa N^2}{3a_0^4} \cos^2 \left[\frac{\beta}{\beta_c} \arccos \left(\frac{a_0^2}{\tau^2} \right) \right], \end{aligned} \quad (10)$$

where β_c denotes the critical value of the dilaton coupling above which no solution exists, with

$$a_0^4 = \frac{\kappa N^2}{3} \cos^2 \left(\frac{\pi \beta}{2\beta_c} \right), \quad 0 \leq \beta < \beta_c = \frac{2\sqrt{2}}{\sqrt{3}}. \quad (11)$$

The action of this wormhole can be easily calculated and reads

¹This fact that the wormhole action could be negative for some potentials was already noticed in [29].

$$S_{\text{GS}}^{(\beta)} = 2\pi^2 \int_{a_0}^{\infty} d\tau \frac{2N^2 e^{-\beta\phi\sqrt{\kappa}}}{\tau^3 \sqrt{1 - \frac{a_0^4}{\tau^4}}} = \frac{4\sqrt{2}\pi^2 N}{\beta\sqrt{\kappa}} \sin\left(\frac{\pi\beta}{2\beta_c}\right). \quad (12)$$

In the limit $\beta \rightarrow 0$, one gets a version of the GS solution without dilaton, whose action is

$$S_{\text{GS}}^{(0)} = \frac{\sqrt{3}\pi^3 N}{\sqrt{\kappa}}. \quad (13)$$

More precisely what we are discussing here is the action of a semiwormhole; to get an action for the whole wormhole with two asymptotic regions we should just multiply this result by a factor of two.²

B. Baby universe interpretation

Euclidean wormholes can be interpreted as tunneling events leading to the creation of baby universes [3,8]. It was noted in [26] that GS wormholes are leading to the materialization of baby universes which are *contracting* after analytic continuation to Minkowski time. Indeed, a regular wormhole at $\tau = 0$ has finite size $a(0) = a_0 \neq 0$, and zero derivative $\dot{a}(0) = 0$ such that for small τ we can expand

$$a(\tau) = a_0 + \frac{1}{2}a_2\tau^2 + \mathcal{O}(\tau^4), \quad (14)$$

where the coefficient $a_2 = \ddot{a}(0)$. After analytic continuation to Minkowski time $t = -i\tau$ we get

$$a(t) = a_0 - \frac{1}{2}a_2t^2 + \mathcal{O}(t^4). \quad (15)$$

Now it is clear that $a_2 > 0$ and $a_2 < 0$ correspond respectively to contracting and expanding small universes. The GS wormhole obviously has $a_2 = \ddot{a}(0) > 0$, since the neck of the wormhole is a minimum of $a(\tau)$. Instead, a wormhole leading to an *expanding* baby universe should have $a_2 = \ddot{a}(0) < 0$, i.e., the ‘‘neck’’ of such a wormhole should be a local maximum. By combining the first two equations of (7), one can see that the axion charge is required so that there can be a local minimum of the scale factor somewhere in the geometry.

C. Initial conditions

The variational problem following from the reduced action (4) is well defined only if the following boundary terms vanish:

$$\left[\frac{3a^2}{h\kappa} \delta\dot{a} \right]_0^{\tau_f} = 0 \quad \text{and} \quad \left[\frac{a^3 \dot{\phi}}{h} \delta\phi \right]_0^{\tau_f} = 0. \quad (16)$$

This is realized at the wormhole neck $\tau = 0$ for the initial conditions $\dot{a}(0) = 0$ and $\dot{\phi}(0) = 0$, and in the asymptotic future for the conditions $\dot{a}(\tau_f) = 1$ and $\phi(\tau_f) = 0$, which imply that the asymptotic future is the flat Euclidean spacetime. This explains why the Gibbons-Hawking-York term must not be added to the action in this case, as it would suppress the boundary term in (4) and consequently would imply that the value of the scale factor a must be fixed at the boundary instead of \dot{a} ; yet fixing \dot{a} is precisely what allows us to reach flat Euclidean spacetime in the asymptotic future as well as impose the wormhole constraint $\dot{a}(0) = 0$ at the origin.

On the classical solution, we must also specify the initial values of the scale factor and scalar field. The value of the scalar field $\phi(0) = \phi_0$ is a free parameter, while the throat size, $a(0) = a_0$, is determined by the Friedmann constraint at $\tau = 0$:

$$1 = \frac{\kappa}{3} \left(a_0^2 V(\phi_0) + \frac{Q^2}{a_0^4} \right), \quad (17)$$

$$\Leftrightarrow \frac{\kappa}{3} V(\phi_0) x^3 - x^2 + \frac{\kappa Q^2}{3} = 0, \quad x = a_0^2, \quad (18)$$

where we defined

$$Q^2 = N^2 e^{-\beta\phi_0\sqrt{\kappa}}. \quad (19)$$

The discriminant of the cubic equation (18) is $\Delta = \frac{\kappa Q^2}{3} (4 - \kappa^3 Q^2 V(\phi_0)^2)$. When $\Delta > 0$, there are three real solutions for x , while when $\Delta < 0$, there are one real and two complex solutions for x . For $\Delta > 0$ we may equivalently require

$$\frac{2}{Q} > \kappa^{3/2} V(\phi_0). \quad (20)$$

The three solutions can be constructed as follows. Let us define an angle $\theta \in [0, \pi]$ such that

$$\begin{aligned} \cos \theta &= 1 - \frac{1}{2} \kappa^3 Q^2 V^2(\phi_0), \\ \theta &= \arccos \left(1 - \frac{1}{2} \kappa^3 Q^2 V^2(\phi_0) \right). \end{aligned} \quad (21)$$

Then the solutions to Eq. (18) are given by

$$x_j = \frac{1}{\kappa V(\phi_0)} \left(1 + 2 \cos \left(\frac{\theta - 2\pi \cdot j}{3} \right) \right) \quad \text{for } j = 0, 1, 2. \quad (22)$$

Whatever the value of $\theta \in (0, \pi)$, if $V(\phi_0) > 0$ there are always two of these solutions which are positive ($j = 0, 1$) and one which is negative ($j = 2$). From the two positive

²The addition of fermionic zero modes was studied in [30].

solutions for x , we get four real solutions for a_0 , two positive and two negative. The largest positive solution for a_0 satisfies

$$\sqrt{\frac{2}{\kappa V(\phi_0)}} < a_0^{(1)} < \sqrt{\frac{3}{\kappa V(\phi_0)}}, \quad (23)$$

so combining the left inequality with (20), we find $(a_0^{(1)})^2 > \kappa^{1/2} Q$. Therefore

$$\ddot{a}(0) = -\frac{1}{a_0^{(1)}} \left(1 - \frac{\kappa Q^2}{(a_0^{(1)})^4} \right) < 0, \quad (24)$$

i.e. $\frac{d^2 a}{dt^2}(0) = -\ddot{a}(0) > 0$, in other words the solution with largest a_0 corresponds to a “wineglass” wormhole leading to an expanding baby universe. This is the $j = 0$ solution. Assuming $y = \kappa^3 Q^2 V(\phi_0)^2 \ll 1$, we find that $\theta \simeq \pi$ so that $a_0^{(1)} \simeq \sqrt{\frac{3}{\kappa V(\phi_0)}}$, which implies that the throat size is given by the Hubble scale. Meanwhile, the smaller ($j = 1$) root in (22) leads to wormholes of GS type, with the scale factor being a local minimum at the origin.

For $\Delta < 0$, the Eq. (18) only possesses one real root, which reads:

$$x_0 = \frac{1}{\kappa V(\phi_0)} \left[1 - 2 \cosh \left(\frac{1}{3} \cosh^{-1} \left(\frac{\kappa^3 Q^2 V(\phi_0)^2}{2} - 1 \right) \right) \right]. \quad (25)$$

Because $\Delta < 0$, the arc-hyperbolic cosine in this expression is real, so x_0 is real and negative. The corresponding solution for a_0 is thus imaginary and can be discarded.

Therefore, $\Delta > 0$ is a necessary (but not sufficient) condition on the parameter space for obtaining a wormhole solution.

III. AXION-DILATON WORMHOLES

After these preliminaries, we are ready to search for wormhole solutions. We will start with the case of the axion-dilaton-gravity system, where we assume the dilaton to be massive, that is to say we choose the potential

$$V(\phi) = \frac{1}{2} m^2 \phi^2, \quad (26)$$

where m is the dilaton mass. The equations of motion (7) in the gauge $h = 1$ now read

$$\begin{cases} 2a\ddot{a} + \dot{a}^2 - 1 + \kappa a^2 \left(\frac{\dot{\phi}^2}{2} + \frac{1}{2} m^2 \phi^2 \right) - \frac{\kappa N^2}{a^4} e^{-\beta\phi\sqrt{\kappa}} = 0 & \text{(acceleration equation),} \\ \dot{a}^2 - 1 = \frac{\kappa a^2}{3} \left(\frac{\dot{\phi}^2}{2} - \frac{1}{2} m^2 \phi^2 \right) - \frac{\kappa N^2}{3a^4} e^{-\beta\phi\sqrt{\kappa}} & \text{(Friedmann constraint),} \\ \ddot{\phi} + \frac{3\dot{a}}{a} \dot{\phi} = m^2 \phi - \frac{\beta N^2 \sqrt{\kappa}}{a^6} e^{-\beta\phi\sqrt{\kappa}} & \text{(dilaton equation).} \end{cases} \quad (27)$$

The dilaton equation in (27) possesses a mechanical analogy as the motion of a *particle* $\phi(\tau)$ in an *effective potential* $W(\phi)$:

$$W(\phi) = -V(\phi) - \frac{N^2}{a^6} e^{-\beta\phi\sqrt{\kappa}}, \quad (28)$$

$$\frac{dW(\phi)}{d\phi} = -m^2 \phi + \frac{\beta N^2 \sqrt{\kappa}}{a^6} e^{-\beta\phi\sqrt{\kappa}}. \quad (29)$$

We see that the fate of the particle released at some point $\phi(0) = \phi_0 > 0$ with zero velocity $\dot{\phi}(0) = 0$ depends on the sign of $W_{,\phi}$ at this point. Depending on which term in the potential $W(\phi)$ dominates at this point, the particle either starts to move to the right (increasing ϕ) or to the left (decreasing ϕ). Since we want to obtain an asymptotically flat geometry, for $\tau \rightarrow \infty$ the dilaton field should eventually settle at its vacuum value $\phi = 0$. The shape of the effective potential crucially depends on the axion charge N , and also on which root is chosen in (22)—see Fig. 3 for an illustration. One feature that becomes immediately clear

upon inspection of the effective potential is that solutions in which the dilaton monotonically rolls down its potential can only exist in very limited parameter ranges, precisely in the regions near the gap seen in the right-hand plot. This property is useful in the numerical search for solutions, to which we now turn.

A. Generalizations of Giddings-Strominger wormholes

We will first concentrate on generalizations of the GS solution (by which we mean wormholes leading to the nucleation of contracting baby universes), in the presence of a massive dilaton. This type of solution was already discussed in the recent work [22], though our search is more comprehensive and we find numerous additional solutions here. In [22], it was shown that solutions only depend on the combination of parameters $m^2 q/f$ and β , a result which follows from the possible field rescalings which we review in Appendix B. The authors of [22] fixed $q/f = \sqrt{2} \Leftrightarrow N = 1$ and varied m . Instead, in our numerical analysis we have fixed $m = 10^{-2}$ and varied N . The two

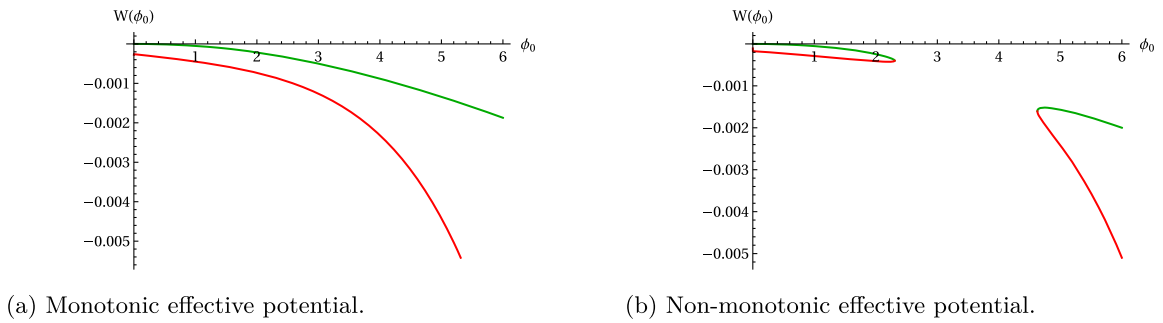


FIG. 3. Effective potential $W(\phi)$ as a function of ϕ_0 for axion charge $N = 20,000$ (left) and $N = 30,000$ (right). The other parameters are the same for both plots: $m = 0.01$ and $\beta = 1.2$. The green line corresponds to the large root in (22), while the red line corresponds to the smaller positive root. The plot on the right contains a gap, which is caused by there existing no real solutions to the cubic equation (18) in that range.

procedures are exactly equivalent, note however that in [22] they use a different, noncanonical definition of the dilaton potential so that their mass is rescaled, $m_{\text{there}} = m_{\text{here}}/\sqrt{2}$, compared to ours.

In looking for solutions, we search for domains of the initial dilaton value ϕ_0 in which we can identify an over-/undershooting behavior of the solution. By this we mean that we look for values of ϕ_0 such that small changes cause the asymptotic value of the dilaton to switch between running off to plus or minus infinity. Then we can infer, by continuity, that somewhere in between a solution must exist in which the dilaton approaches $\phi = 0$ asymptotically. We may hone in on the actual solution to the desired level of accuracy (which is typically at the level of about 20 significant digits, sometimes more) with an optimization algorithm. Here a Newtonian algorithm suffices. In finding appropriate initial ranges of ϕ_0 , we take guidance from the effective potential, as discussed above.

The first examples of solutions are shown in Fig. 4. These solutions all have the same dilaton coupling $\beta = 1.2$, and the same axion charge $N = 30,000$, so that $m^2 N = 3$.

For all solutions, the origin $a(0)$ represents a local minimum of the scale factor, which is why these wormholes would nucleate contracting universes. In [22] only solutions analogous to the first, monotonic solution with $\phi_0 \approx 0.71$ were found. Remarkably, with increasing ϕ_0 , we find additional solutions in which the field evolutions become more intricate, and oscillations develop. It is noteworthy that both the dilaton and the scale factor develop these oscillations (in contrast to the oscillating bounces of [31], in which only the scalar field oscillates). In the figure we show four examples, although we did not encounter any obstruction when searching for solutions with ever larger ϕ_0 and more numerous oscillations—we suspect that there exists no upper limit to the number of oscillations.

The Euclidean action of these solutions is shown in Fig. 5, both as a function of the radial coordinate τ and in terms of the final asymptotic values. One can see that the action integral only receives significant contributions as long as the dilaton is evolving noticeably. Once the dilaton settles in its potential minimum and the geometry approaches that of flat space, the action stabilises.

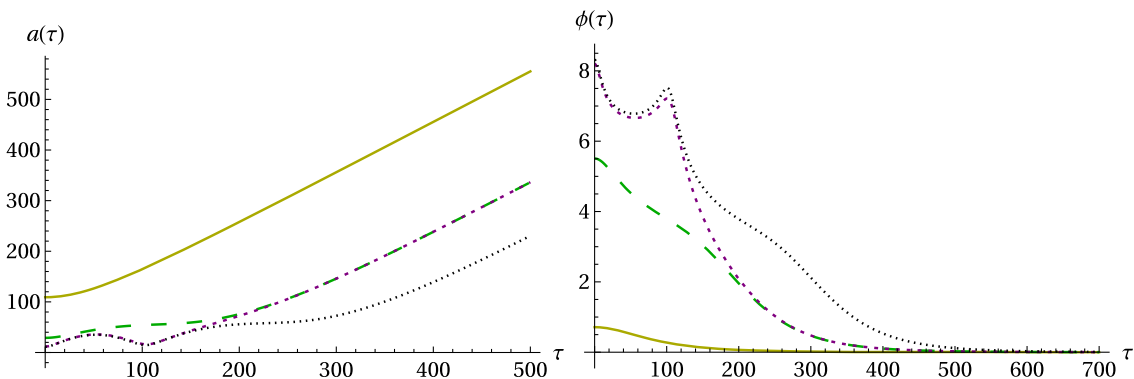


FIG. 4. Wormhole solutions with a massive dilaton, with the scale factor shown on the left and the dilaton evolution on the right. All solutions have $\kappa = 1$, $\beta = 1.2$, $N = 30,000$, $m = 0.01$. The individual solutions are characterized by the initial value of the dilaton, given respectively by the values $\phi_0 = 0.7118165858$, 5.5075291704 , 8.1964321797 , 8.3116654157 (we indicate a number of significant digits such that the action can be determined to better than percent level accuracy). Solutions with larger ϕ_0 display a more intricate field evolution, containing oscillations of the fields.

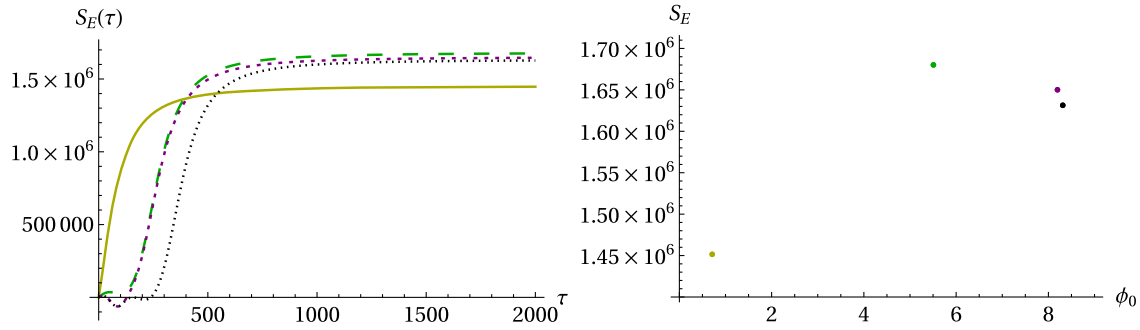


FIG. 5. The Euclidean action, as a function of τ (left plot) and a graph with the asymptotic values (right plot), for the solutions shown in Fig. 4. Intriguingly, the action is not monotonic in ϕ_0 , but starts decreasing as more oscillations are added.

To obtain the asymptotic value, we have added an analytically calculable remainder (as explained in Appendix C), which ensures that the end result is trustworthy up to a known level of precision. The most obvious feature is that the action is positive, in line with the interpretation of these solutions as mediating the nucleation of baby universe in a tunnelling-type event. The second solution, containing an inflection point in the scale factor, has a higher action. However, what is truly surprising, is that for the solutions with additional features, in particular the presence of one or two additional minima in $a(\tau)$, the action decreases again. Assuming the probability of nucleation per unit four-volume to be given approximately by $e^{-2S_E/\hbar}$, one would conclude that solutions with additional oscillations are more likely to occur than those with fewer such features. This surprising property requires further explanation. Notice however, for now, that the simplest, monotonic solution appears to be the most likely overall, though in the absence of analytic expressions for these solutions we cannot be sure what happens to the action in the limit of infinite numbers of field oscillations. In particular, we cannot assess whether in this limit the action would remain above that of the lowest ϕ_0 solution.

We can also look at solutions at a larger value of the dilaton coupling—Fig. 6 shows an example with $\beta = 1.58$ and with charge $N = 47,089$ (the reason for choosing this peculiar looking number will become clear below). At these parameter values we find a total of five GS-type solutions, containing a single minimum in the scale factor, that is to say only the minimum at the origin. The figure then also contains a solution with two minima, at an even larger dilaton value ϕ_0 . The action of these solutions is shown in Fig. 7. We notice the same feature as before, namely that the action first increases with the complexity of the solutions (and with increasing ϕ_0) but then starts to decrease again. This time the effect is even more pronounced, and the solution with two minima of the scale factor already has a Euclidean action that lies below that of the lowest ϕ_0 solution. We will discuss this puzzling feature further in later parts of the paper.

The existence of these generalized GS-solutions depends on the parameters m^2N and β , as well as on the initial dilaton values ϕ_0 , in a remarkably intricate way. We illustrate this first with the simplified plot in Fig. 8, and then with the more complete (but at first sight somewhat bewildering) plot in Fig. 9. Let us describe the simplified plot first, starting with the light brown curve corresponding

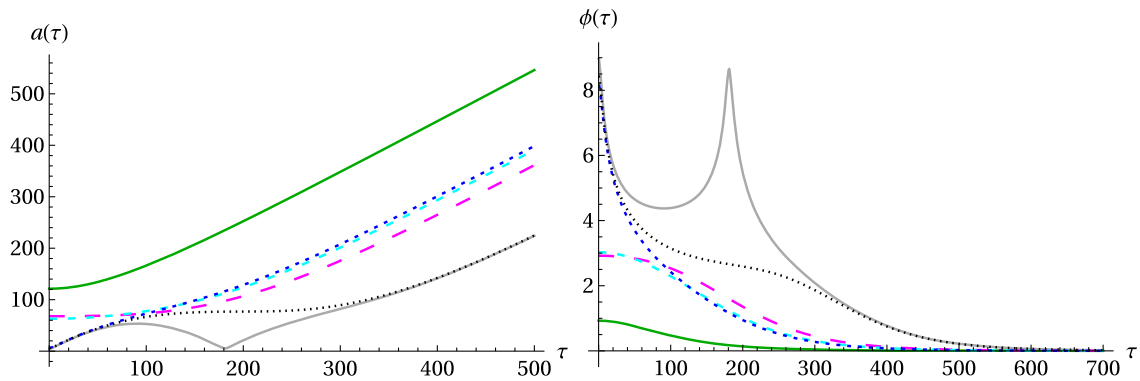


FIG. 6. Wormhole solutions with a massive dilaton, with the scale factor shown on the left and the dilaton evolution on the right. All solutions have $\kappa = 1$, $\beta = 1.58$, $N = 47,089$, $m = 0.01$. The initial dilaton values are $\phi_0 = 0.9267658893, 2.9202136114, 3.0261054894, 8.1578681214, 8.4314038628, 8.9744628254$. Solutions with larger ϕ_0 again display oscillations of the fields.

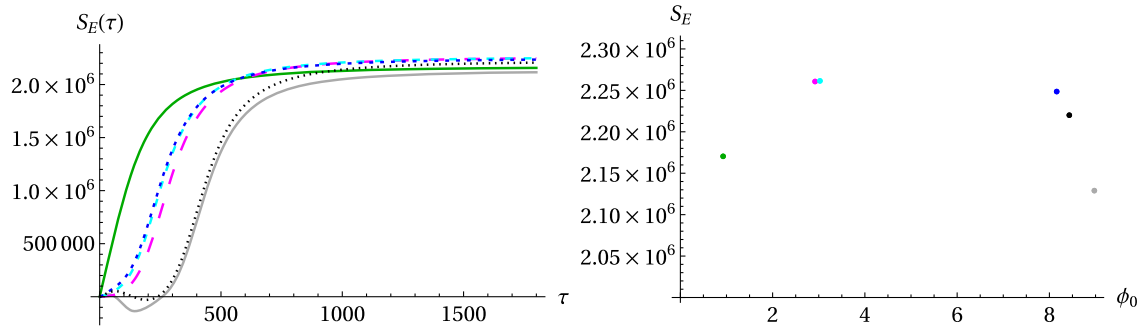


FIG. 7. The Euclidean action, as a function of τ (left plot) and a graph with the asymptotic values (right plot), for the solutions shown in Fig. 6. Again, the action is not monotonic in ϕ_0 , but starts decreasing as more oscillations are added.

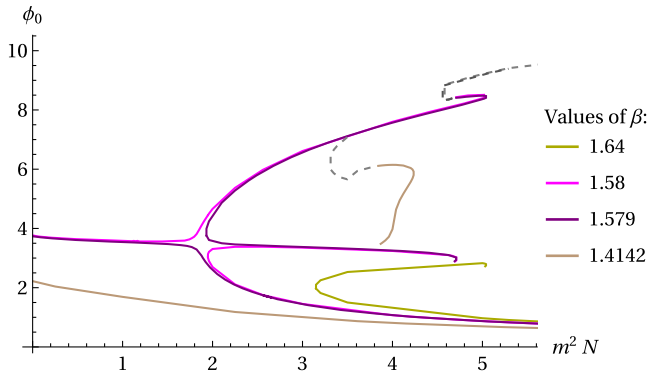


FIG. 8. Branch structure of the generalized GS-type solutions with at most one extra minimum of the scale factor, for four representative values of the dilaton coupling. A full description is provided in the main text.

to $\beta = \sqrt{2} \approx 1.4142$. The lowest curve on the plot shows that wormhole solutions exist for all values of $m^2 N$, i.e. also in the limit of vanishing mass. This is expected, as this value of β lies below the critical GS value $\beta_c = \sqrt{8/3} \approx 1.633$. However, an additional branch of solutions exists, starting around $m^2 N \approx 4$ and $\phi_0 \approx 4$. The starting value of

this new branch is not arbitrary: it corresponds to the onset of the “gap” in the effective potential $W(\phi)$, as explained in and above Fig. 3. Along this new branch lie the solutions with inflection points and oscillations in the fields. In fact, as one moves along the branch, the solutions become progressively more complicated. The solid light brown curve includes all solutions (with $\beta = \sqrt{2}$) that have a single minimum in the scale factor. The dashed extension of the curve indicates that further solutions, with two and more minima of the scale factor, exist as one moves in the broad direction of larger ϕ_0 values. In fact, as far as we can tell by our numerical investigations, the curve keeps moving up in a zigzag manner, without apparent limit.

This behavior is analogous for all values of β below a certain β_i , with $1.579 < \beta_i < 1.58$, at which value an “inversion” of the branch structure takes place. Indeed, the pink curve ($\beta = 1.58$) that links to the vertical axis at $m = 0$ now moves up to larger ϕ_0 values around $m^2 N \approx 2$, and the new branch of solutions appears below, at smaller ϕ_0 . Now it is the original branch that continues upwards in a zigzag manner, indicated by the dashed extension of the solid line, leading to ever more involved field evolutions. By contrast, the new branch that appears around $m^2 N \approx 2$ has a bifurcating pattern. Following it along the larger ϕ_0

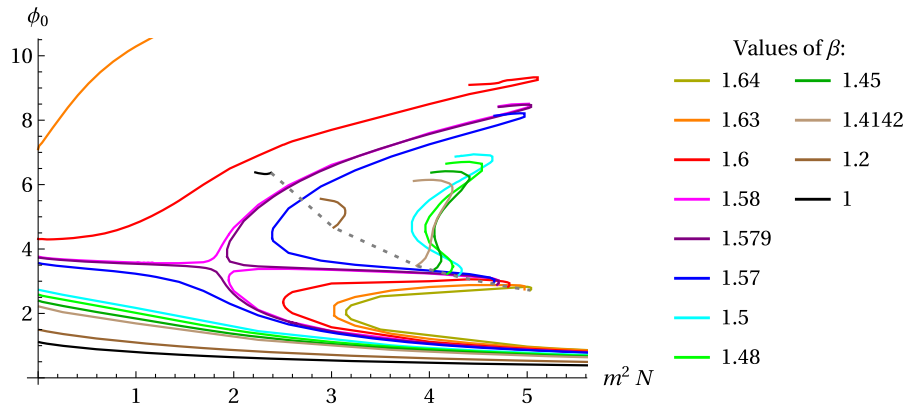


FIG. 9. A more complete version of the plot shown in Fig. 8, containing curves at additional values of the dilaton coupling β . The inversion of the branch structure above β_i (i.e., for the curves with $\beta \geq 1.58$) is clearly visible. See the main text for a detailed analysis.

values, it has an end point at $m^2N \approx 4.8$ and $\phi_0 \approx 3$, corresponding to the (dis)appearance of the gap in the effective potential $W(\phi)$. Following this curve in the other direction, one finds solutions with ever larger m^2N , again presumably without limiting m^2N value. The solutions shown in Fig. 6 present a vertical slice through these curves, and from Fig. 8 one can see that choosing m^2N to lie a little below 4.8 allows one to pick up the maximal variety of solutions.

If we increase the dilaton coupling β further, then on the vertical axis, at zero dilaton mass, the required ϕ_0 values keep increasing and tend to infinity as the critical value $\beta_c = \sqrt{8/3} \approx 1.633$ is reached. This is the limit found by Giddings and Strominger for the massless case. Beyond this value, the line that connects to the vertical axis thus disappears. Consider for instance the light green curve at $\beta = 1.64$ in Fig. 8. At this value, only the new bifurcating branch of the type described above exists. For this value of β , it appears around $m^2N \approx 3.2$, and this implies that GS-type wormhole solutions only exist for masses/charges above this value.

We can now take a look at the more complete plot shown in Fig. 9. One can make out very well the similarities between all curves with $\beta < \beta_i$, and the inverted structure at larger coupling. For completeness, one should picture the upper branches (for $\beta < \beta_i$) as continuing in the described zigzag pattern to larger ϕ_0 values. The dashed line in the figure corresponds to the combination of m^2N and ϕ_0 values at which the gap in the effective potential appears, i.e., the dashed line is the locus of end points of the new branches. The fact that an inversion of the branch structure occurs as β is increased is made plausible by the fact that the curve that connects to zero mass must disappear entirely once β surpasses β_c . However, this argument is not sufficient to determine the precise value β_i of the dilaton coupling at which the inversion occurs. This is an open problem, the resolution of which will likely require at least a partially analytic understanding of these numerically found solutions.

Connected to the above point is the realization that GS-type wormholes in fact exist at $\beta > \beta_c$, but only with a sufficiently large mass and charge. This fact was already discovered in [22]. Figure 10 makes this notion more precise, by plotting the required minimum values of m^2N as a function of β . The discontinuous jump at β_c is precisely due to the appearance of new branches disconnected from the vertical $m^2N = 0$ axis. The obvious implication of this plot is that the required m^2N value becomes ever larger as the dilaton coupling is increased, with the approximate linear relation

$$(m^2N)_{\min} \approx 10.8\beta - 14.6, \quad (30)$$

valid for $\beta \geq \beta_c$.

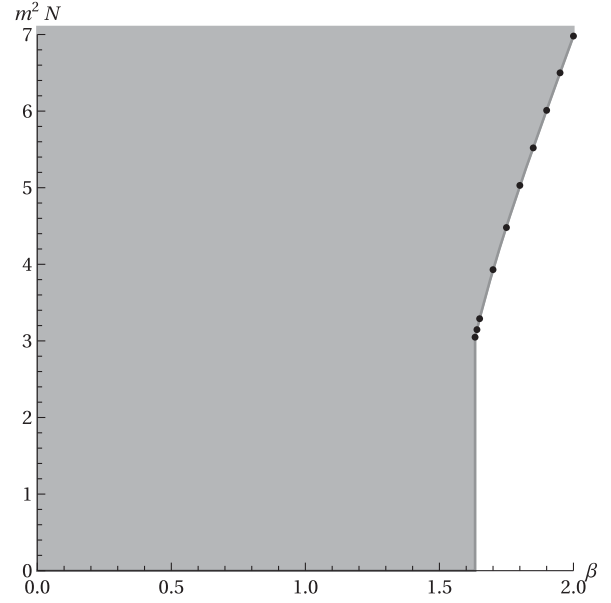


FIG. 10. Minimal mass/charge m^2N as a function of β for generalized GS-type solutions.

B. Wormholes leading to expanding baby universes

The same axion-dilaton-gravity theory with massive dilaton admits another type of wormhole solution, in which the origin $a(0)$ corresponds to a local maximum of the scale factor. As described in Sec. II B, if we interpret such solutions as mediating the nucleation of baby universes, then this feature leads to baby universes that are expanding (in Lorentzian time), a feature that may allow them to become large and be long lived. We will loosely refer to such solutions as *expanding wormholes*. The methods used to find such expanding wormholes are the same as those described in the previous section, except that in fixing initial conditions, we must always choose the largest root of the cubic equation (18), as explained in Sec. II C.

A first example of such a wormhole is shown in Fig. 11. One can only make out the local maximum of the scale factor at the origin by zooming in, see the inset in the left panel in the figure. For this solution, the dilaton rolls down monotonically in its potential, asymptotically settling at its minimum. The Euclidean action is positive, in line with the interpretation of this solution as mediating a tunneling event.

With the same parameters, there exist additional solutions at larger initial dilaton values, see Fig. 12. These solutions are reminiscent of the solutions with oscillations in the fields, discovered also for GS-type wormholes in the previous section. A distinction here is that in these more involved solutions the dilaton first runs up its potential, before turning around and (perhaps after several additional oscillations) eventually settling in its potential minimum. Associated with these oscillations of the dilaton is an additional “breathing” behavior of the scale factor, which

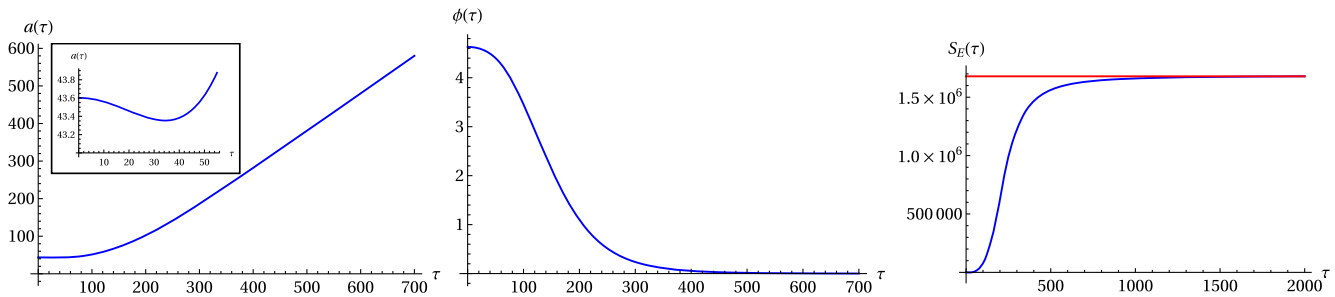


FIG. 11. An example of a wormhole leading to an expanding universe upon analytic continuation. For this solution, the dilaton rolls down the potential monotonically. Shown are the scale factor (left), dilaton (middle) and Euclidean action (right). The red line represents the value of the final Euclidean action when taking the analytic remainder into account (see Appendix C). The parameter values are $m = 0.01$, $\beta = 1.2$, $N = 30,000$ and the initial dilaton value is $\phi_0 = 4.6297956230$.

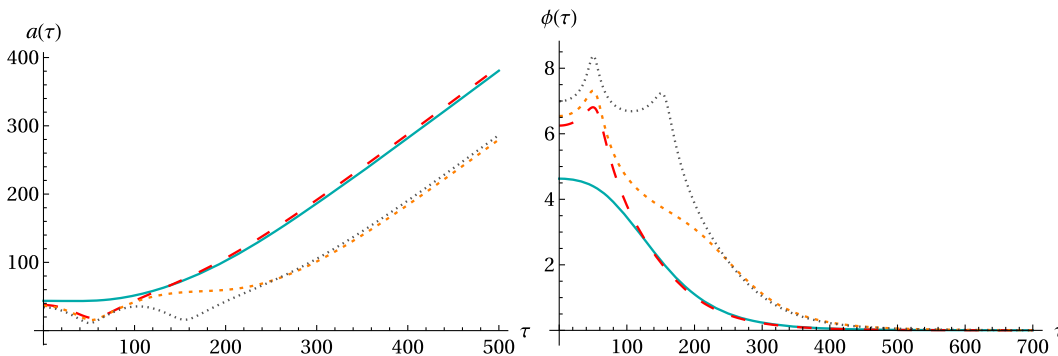


FIG. 12. Expanding wormhole solutions with a massive dilaton, with the scale factor shown on the left and the dilaton evolution on the right. All solutions have $\kappa = 1$, $\beta = 1.2$, $N = 30,000$, $m = 0.01$. The individual solutions are characterized by the initial value of the dilaton, given respectively by the values $\phi_0 = 4.6297956230$, 6.2498081147 , 6.5411315634 , 6.9914512133 . Solutions with larger ϕ_0 display a more intricate field evolution, containing oscillations of the fields.

may expand and shrink alternately before eventually tending to flat space at large radii.

The action for these expanding wormholes is shown in Fig. 13, on the left as a function of radius and on the right in terms of the asymptotic values. This time, in contrast with Fig. 5, the action immediately starts decreasing as the solutions progressively develop additional inflection points and oscillations. This unusual feature complicates the interpretation of these solutions, as it naively suggests that

expanding wormholes with more oscillations are more likely than those with fewer features. We will comment further on this peculiarity in the discussion section. Similar features occur at other values of the dilaton coupling, see Figs. 14 and 15 for additional examples.

We can now try to gain a more global understanding of the existence of expanding wormhole solutions. The existence of solutions as a function of m^2N and ϕ_0 , for various values of the coupling β , is shown in Fig. 16.

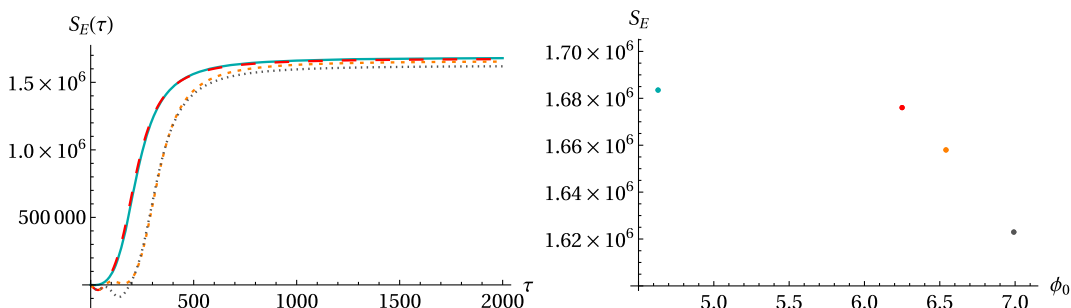


FIG. 13. The Euclidean action, as a function of τ (left plot) and a graph with the asymptotic values (right plot), for the solutions shown in Fig. 12. Surprisingly, the action decreases as the field evolutions become more involved.

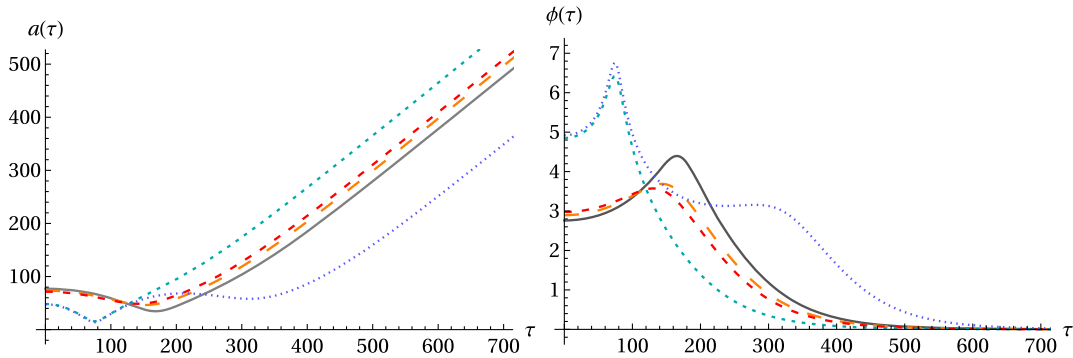


FIG. 14. Expanding wormholes with dilaton coupling $\beta = 1.4$ and $m^2N = 3.525$. The initial dilaton values are $\phi_0 = 2.7593083935, 2.8947797102, 2.9770027664, 4.8514743456, 4.9204400124$.

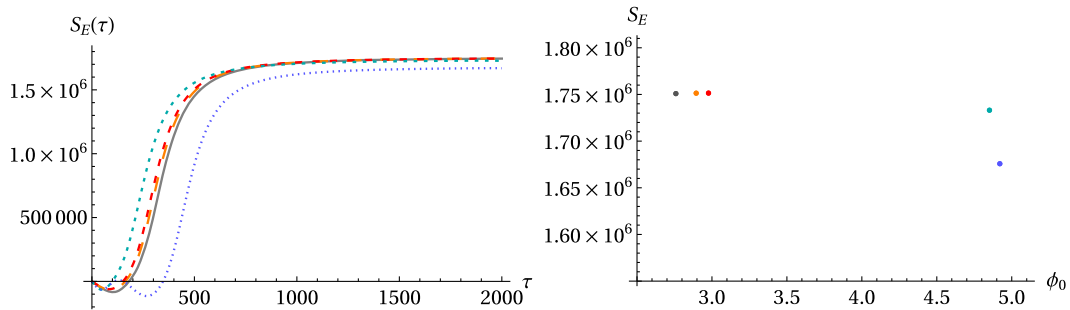


FIG. 15. The Euclidean action of the solutions shown in Fig. 14. Once again, the solutions with additional oscillations have lower Euclidean action.

The first impression that one obtains is that, unlike for generalized GS-type wormholes, the behavior is qualitatively similar for different β values. In this case, no solutions exist at zero mass, hence we do not expect (and do not see) branches connecting to the vertical axis. However, at sufficiently large m^2N branches of solutions develop, starting at values at which a gap in the effective potential $W(\phi)$ appears, in analogy with the GS-type solutions and as discussed in connection with Fig. 3.

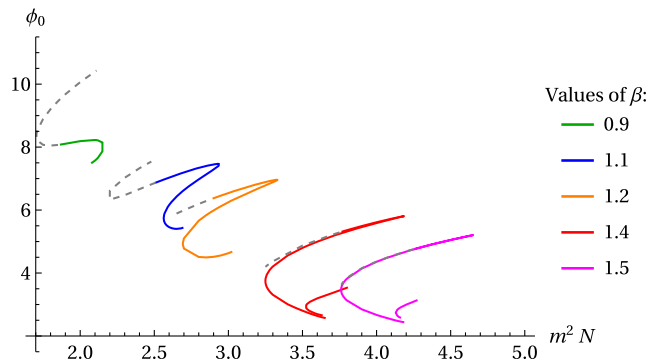


FIG. 16. Summary plot of the existence of expanding wormholes, as a function of the mass/charge combination m^2N and the initial dilaton values ϕ_0 , for various values of the dilaton coupling β . A detailed description is provided in the main text.

These branches then continue in a rough zigzag fashion toward larger ϕ_0 values. As they do so, the solutions become progressively more intricate, developing inflection points and then additional oscillations. The dashed lines indicate parameter regions where an additional minimum in the scale factor exists, and one should picture the branches as continuing upwards indefinitely, with the solutions containing ever greater numbers of oscillations.

Two examples of series of solutions, which show how additional features form, are provided in Figs. 17 and 18. In the first case, we see how the dilaton starts changing its initial direction of evolution. In the second case, we see how an additional minimum in the scale factor develops. In both series, it is again made manifest that additional features lower the action.

One feature which we have not mentioned yet is that for large enough dilaton coupling (approximately $\beta > 1.3$) a second branch of solutions forms, see the examples with $\beta = 1.4, 1.5$ in Fig. 16. These additional branches are again bifurcating, ending on both sides at the locations where the effective potential stops developing a gap. The expanding wormhole solutions belonging to these branches are however very similar to those in the first branch. In fact, we already saw examples of solutions belonging to a second branch in Figs. 14 and 15—these were the solutions with $\phi_0 \approx 2.89, 2.97$. These figures indicate that the various

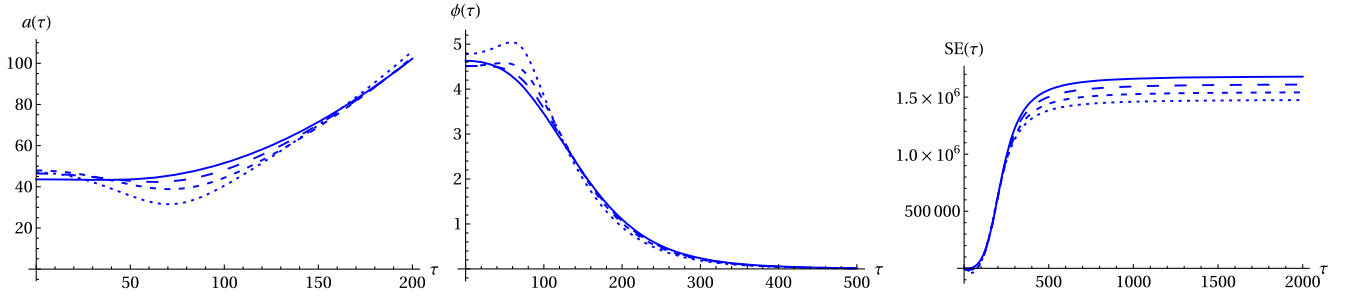


FIG. 17. Transition from a solution with a monotonically evolving dilaton to a solution with an oscillating dilaton, with parameter values $\beta = 1.2$ and $N = 30,000$ to $27,000$, the smaller values of N corresponding to the more finely dashed curves.

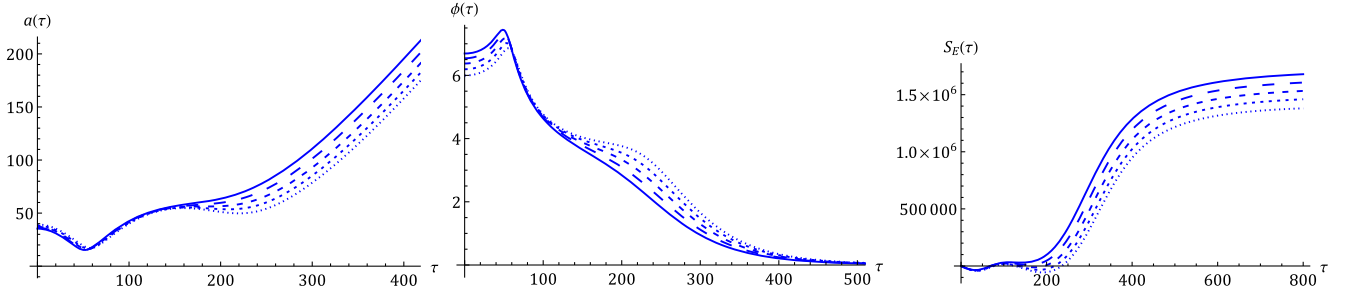


FIG. 18. Transition from a solution with a single minimum of the scale factor to one with two minima. The parameter values are $m = 0.01$, $\beta = 1.2$ and $N = 31,000$, $\phi_0 = 6.6921845703$; $N = 30,000$, $\phi_0 = 6.5411318359$; $N = 29,000$, $\phi_0 = 6.3756220703$; $N = 28,000$, $\phi_0 = 6.1942070312$; $N = 27,000$, $\phi_0 = 5.9951564438$ (smaller values of N correspond to more finely dashed curves).

solutions evolve continuously with the initial value ϕ_0 , and that no significant physical distinction between the branches is noticeable. We should also highlight that there appears to exist no upper bound on the dilaton coupling β . Although solutions do become harder to find numerically at large β , we see no evidence for any obstruction at large β —for illustration, we provide an example of an expanding wormhole with $\beta = 2$ in Fig. 19. The existence of solutions at large dilaton coupling may be of interest in string theory models, where it is rather natural to obtain dilaton couplings of order unity.

Figure 20 explores a further physical aspect of the solutions, namely their action-to-charge ratio. As the figure

indicates, this is found to be a monotonically increasing function of the charge N (with fixed mass m), which points to the fact that the expanding wormhole solutions might be nonperturbatively unstable, as it would be preferable for a fixed charge wormhole to break up into two smaller wormholes with combined charge equal to the original one [22], as long as appropriate solutions with smaller m^2N actually exist (Fig. 16 indicates that if they exist, they must contain a large number of oscillations). We should note however that determining the rate of this process would require knowledge of interpolating solutions linking the initial and final configurations. We leave this topic for future research.

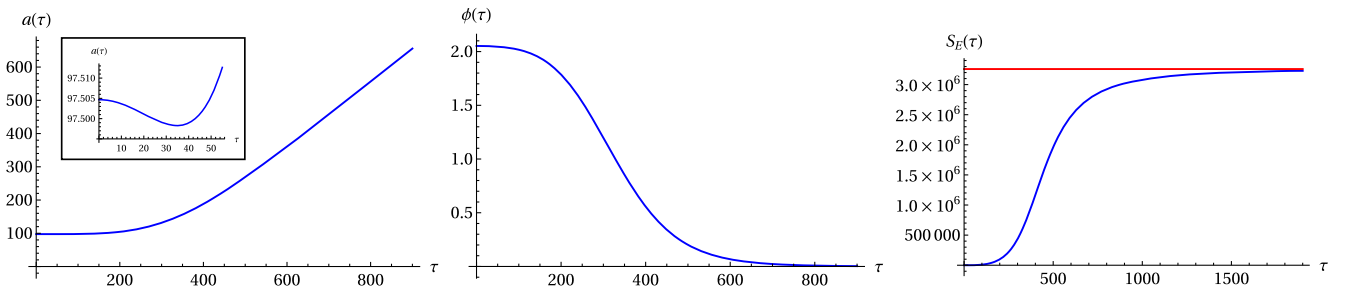


FIG. 19. An example of a wormhole with large dilaton coupling, in this case $\beta = 2$. Shown are again the scale factor (left), dilaton (middle), and Euclidean action (right). The parameter values are $m = 0.01$, $\beta = 2$, $N = 73,940$ and the initial dilaton value is $\phi_0 = 2.0522333714$.

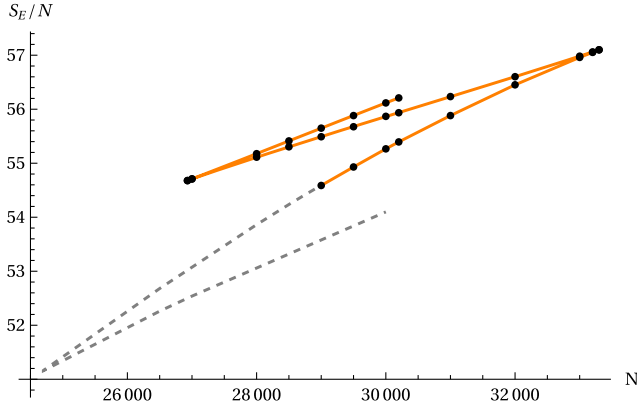


FIG. 20. The action-to-charge ratio for expanding wormholes with $\beta = 1.2$. The dashed line represents solutions that contain a second minimum in the scale factor, cf., also the $\beta = 1.2$ locus in Fig. 16. In all cases, the action-to-charge ratio increases with increasing charge.

Finally, we may compare GS-type and expanding wormholes, at fixed parameter values. This is done in Fig. 21. As one can see in this picture, the different types of solutions exist at nearby initial values of the dilaton, and in fact even the values of the Euclidean action are intertwined. Overall, the simplest solution, i.e., the GS-type solution with monotonically evolving dilaton, appears to have the lowest action. However, as we cannot extrapolate our results to large numbers of oscillations in the fields, it remains an open question whether this solution is truly the most dominant one. At larger values of the dilaton coupling,

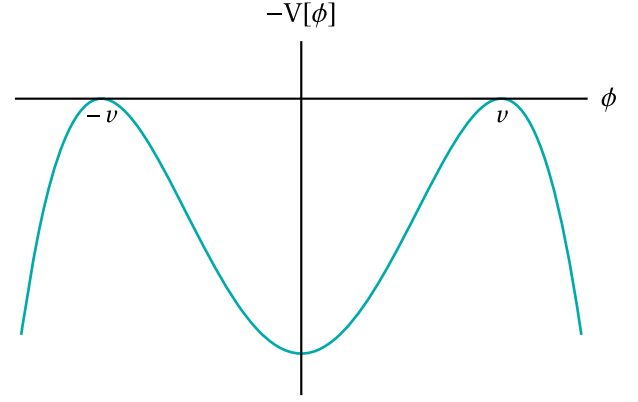


FIG. 22. Symmetric double well potential for the parameter values $\lambda = 0.01$ and $v = 0.4$.

we already know that the simplest solution is not the one with the lowest action, cf., Fig. 7. This is an interesting puzzle requiring future work, and we will provide some comments related to this question in the discussion section.

IV. AXION-SCALAR WORMHOLES LEADING TO EXPANDING BABY UNIVERSES

In the previous section, we saw that the dilaton coupling had a significant effect on the existence and properties of wormhole solutions. One might wonder if solutions also exist without the special dilatonic coupling, i.e., in the presence of an ordinary scalar field. Thus we will set $\beta = 0$, but we will keep the letter ϕ to designate the scalar. The equations of motion (7) then read

$$\begin{cases} 2a\ddot{a} + \dot{a}^2 - 1 + \kappa a^2 \left(\frac{\dot{\phi}^2}{2} + V(\phi) \right) - \frac{\kappa N^2}{a^4} = 0 & \text{(acceleration equation),} \\ \dot{a}^2 - 1 = \frac{\kappa a^2}{3} \left(\frac{\dot{\phi}^2}{2} - V(\phi) \right) - \frac{\kappa N^2}{3a^4} & \text{(Friedmann constraint),} \\ \ddot{\phi} + \frac{3\dot{a}}{a} \dot{\phi} = \frac{dV}{d\phi} & \text{(scalar equation).} \end{cases} \quad (31)$$

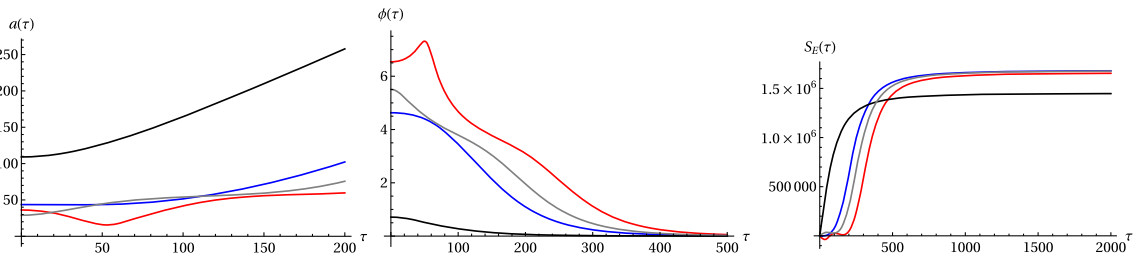


FIG. 21. This figure compares GS-type and expanding wormholes, at the same parameter values $m^2 N = 3$ and dilaton coupling $\beta = 1.2$. The GS-type solutions are depicted by the black ($\phi_0 \approx 0.7$) and gray ($\phi_0 \approx 5.5$) lines. These solutions were already presented in Fig. 4. The blue ($\phi_0 \approx 4.6$) and red ($\phi_0 \approx 6.2$) curves correspond to expanding wormholes, and were shown in Fig. 12. Interestingly, the actions are seen to be quite close to each other, with the gray solution lying in between the two expanding wormhole solutions. It appears that overall the black GS-type solution is dominant, but a verification of this assertion would require an understanding of the infinite oscillation limit of expanding wormholes.

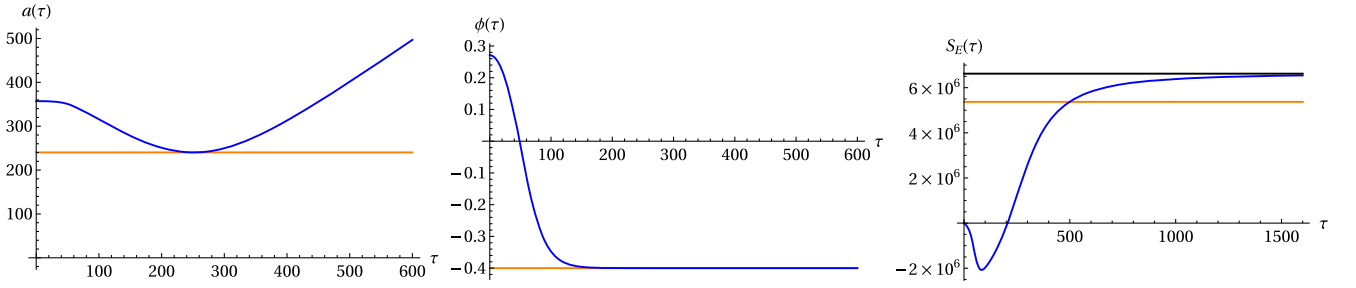


FIG. 23. An example of an expanding wormhole supported by a large axionic charge, and a scalar field in a double well potential. The parameters used are $\lambda = 0.01$, $N = 100000$, $v = 0.4$. The initial scalar field value is $\phi_0 = 0.27112946714882599307$. The orange lines provide the GS wormhole values as reference.

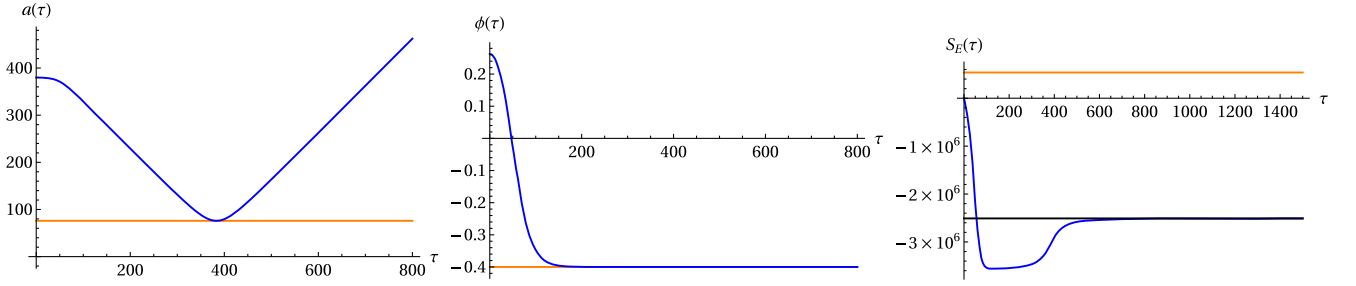


FIG. 24. An example of an expanding wormhole supported by a small axionic charge. The parameters used are $\lambda = 0.01$, $N = 1000$, $v = 0.4$. The initial scalar field values is $\phi_0 = 0.26235021388116072967$.

We will choose the scalar field potential to be of double well form

$$V(\phi) = \frac{1}{4}\lambda(\phi^2 - v^2)^2, \quad (32)$$

where λ is a dimensionless scalar field self-coupling and v is the vacuum expectation value, see Fig. 22. The self-coupling λ may be scaled to any convenient value using the rescalings detailed in Appendix B.³

The scalar field equation in (31) possesses a simple mechanical analogy as the motion of a “particle” in an inverted potential $-V$, under the velocity dependent friction force,

$$F_{\text{friction}} = \frac{3\dot{a}}{a}\dot{\phi}. \quad (33)$$

We see that the friction coefficient could be positive or negative depending on the sign of \dot{a} . Since we are looking for asymptotically flat solutions, the scalar field should approach one of the vacua as $\tau \rightarrow \infty$. Without loss of generality we choose this to be the left vacuum, $\phi = -v$. A particle released with zero velocity will get a chance to reach this vacuum only if it starts at some $\phi_0 \in [0, v]$. Put differently, the potential barrier is required in order to make

the scalar field roll in the appropriate direction after starting with zero velocity. Moreover, the potential minimum is required in order to stabilise the field asymptotically and to approach flat spacetime. For this purpose a single minimum would be enough, but for simplicity (scarcity of free parameters) we choose a symmetric potential here. Typically if ϕ_0 is very close to v we get “overshooting,” since for small τ the scale factor derivative $\dot{a} < 0$ and we have antifriction. Generally with the simple integration of Eq. (31) we can conclude that the work of the friction force has to be compensated by the potential energy [27,34],

$$3 \int_0^\infty d\tau \frac{3\dot{a}}{a} \dot{\phi}^2 = -V(\phi_0). \quad (34)$$

The condition $\Delta > 0$ implies for our symmetric double well potential that:

$$\begin{aligned} 4 - \kappa^3 N^2 \frac{\lambda^2}{16} (\phi_0^2 - v^2)^4 &> 0 \\ \Leftrightarrow (\phi_0^2 - v^2)^4 &< \frac{64}{\kappa^3 N^2 \lambda^2} \\ \Leftrightarrow v^2 - \phi_0^2 &< \frac{2\sqrt{2}}{\kappa^{3/4} \sqrt{N\lambda}}. \end{aligned} \quad (35)$$

³Euclidean solutions in the presence of a double well potential were also studied in, e.g., [32,33].

For $\phi_0 \in [0, v]$, this means that we are restricted to a range of values:

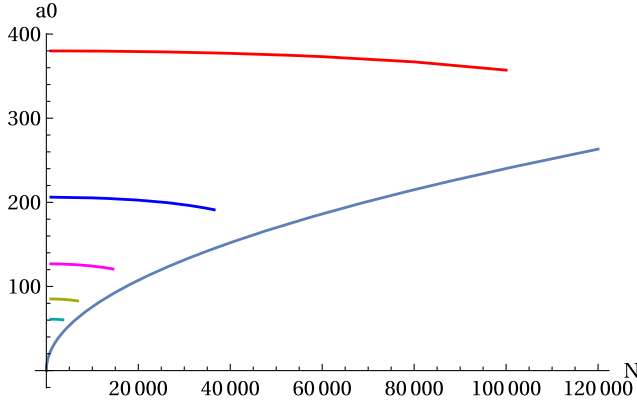


FIG. 25. Wormhole throat size a_0 vs N for the parameter values $\lambda = 0.01$ and $v = 0.4, 0.5, 0.6, 0.7, 0.8$ (going down in the plot). At large N all curves tend to the GS value, shown here by the blue curve.

$$\sqrt{v^2 - \frac{2\sqrt{2}}{\kappa^{3/4}\sqrt{N\lambda}}} < \phi_0 < v. \quad (36)$$

For each set of parameters (v, N) , a wormhole solution is found by fine-tuning the value of ϕ_0 between undershooting and over-shooting values. This implies that, if for the minimal value allowed by the condition (36),

$$\phi_0^{\min} = \sqrt{v^2 - \sqrt{8/(\kappa^{3/2}N\lambda)}}, \quad (37)$$

we have over-shooting, then there will not exist any wormhole solutions. Conversely, if $\phi_0 = \phi_0^{\min}$ leads to undershooting, then there will necessarily exist a wormhole solution. Therefore, for each value of v , the above criterion defines an upper bound on the value of N for which a wormhole solution exists.

Note also that in the symmetric potential Eq. (32) no GS-type wormholes exist with *nontrivial* scalar field. This conclusion can be easily reached by noting that GS-type wormholes have positive \dot{a} , and consequently provide friction in the scalar field equation. So, in order for the

solution to end up on one of the hills (vacua) for $\tau \rightarrow \infty$ one should start rolling down from higher hill, in order to overcome friction, but in a symmetric potential there is no higher hill. We conclude that the only known GS wormholes in this potential arise with a trivial scalar field configuration $\phi = \pm v$.

For the reasons just given we will rather look for wormholes that have a local maximum at the throat, that is to say wormholes that lead to expanding baby universes after analytic continuation to Lorentzian time. The first examples are shown in Figs. 23 and 24, for a large and a small axionic charge respectively. Compared to the dilatonic case, we see that the local maximum at the origin is much more pronounced, and even more so for the small charge solution. The minimum value of the scale factor is found to coincide rather precisely with the GS value (by which we mean the throat size of a GS wormhole, with the scalar residing at a potential minimum), indicated by the orange lines in the figures. In fact, as the charge grows, the initial throat size is reduced, and one may infer that the solutions with larger charge approach GS-type solutions more and more. This is confirmed by a study of the initial throat size as a function of the charge, shown for various potential widths in Fig. 25.

The Euclidean action for these solutions is shown in the right panels of Figs. 23 and 24, as a function of the radial coordinate. One thing we may notice is that it starts off by obtaining negative contributions near the throat. Further away from the throat, as the scalar potential becomes less important (since the scalar approaches the vacuum), the action receives positive contributions. Which contributions dominate depends rather crucially on the axionic charge: the large charge solution ends up having a positive action (in this case larger than the GS value), while the small charge wormhole has a negative Euclidean action. As we will discuss further below, this suggests that only large charge wormholes might be of physical relevance.

Figure 26 shows the action-to-charge ratio for two different potential widths. Just as for the dilatonic case, this ratio is a monotonically increasing function of the

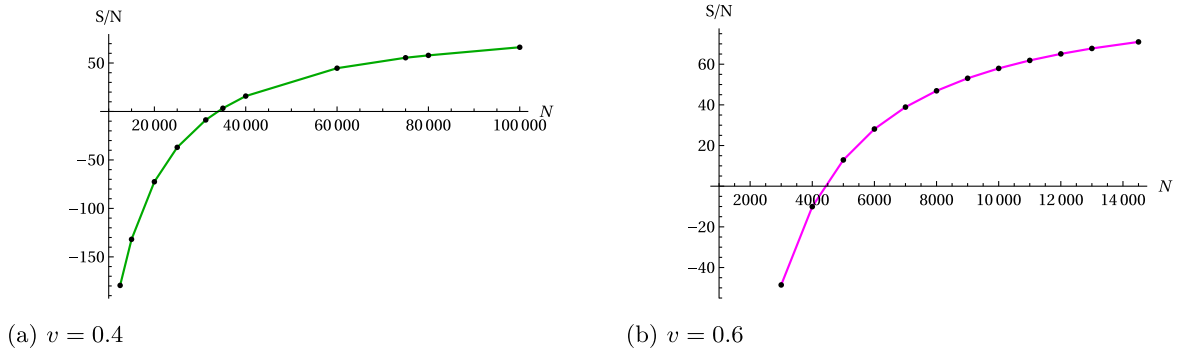


FIG. 26. Plots of the action-to-charge ratio for $v = 0.4$ (left) and $v = 0.6$ (right) with $\lambda = 0.01$.

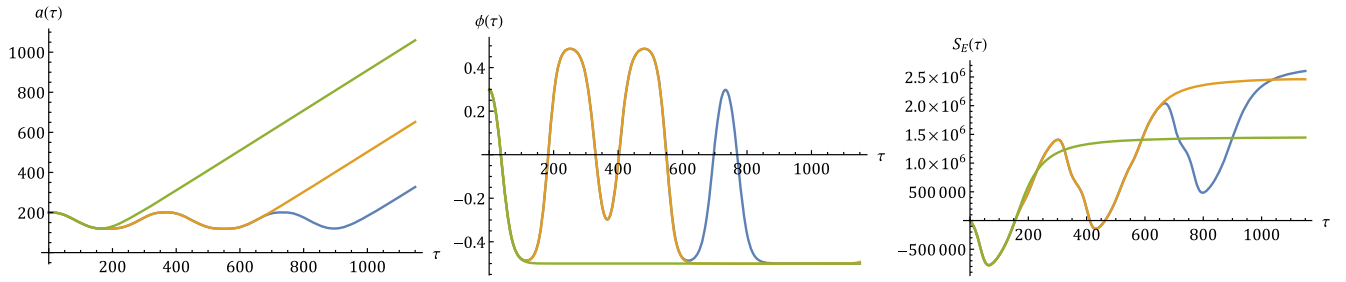


FIG. 27. Comparison of solutions with one, two and three minima for the same theory parameters $N = 25,000$, $\lambda = 0.01$ and $v = 0.5$. The Euclidean action grows with each additional oscillation. The solutions here are specified by initial scalar field values that lie very close to each other, respectively at $\phi_0 = 0.297695980172969317414540$, $0.297530409785421517546558$, $0.297530409646648251937091$ (these solutions must be optimized to high accuracy in order to determine the action reliably).

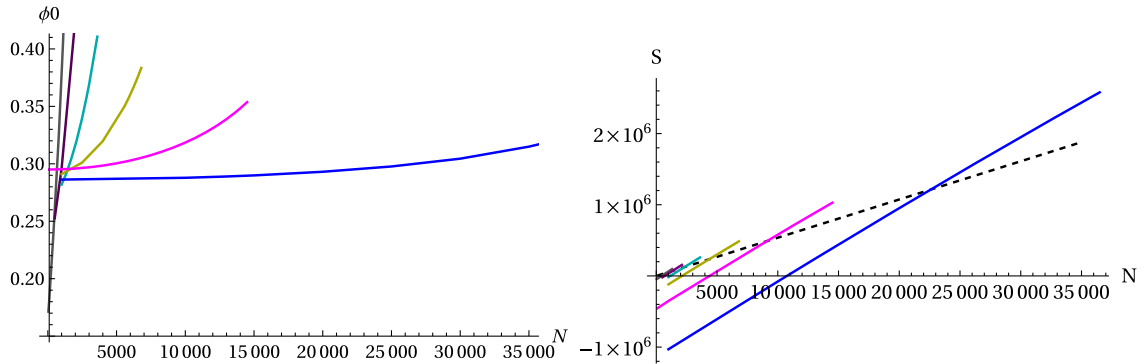


FIG. 28. Summary plots for $v = 1.0$ (black), $v = 0.9$ (purple), $v = 0.8$ (turquoise), $v = 0.7$ (green), $v = 0.6$ (pink), and $v = 0.5$ (blue). Here $\lambda = 0.01$. The right plot shows the most striking result, namely that the action varies linearly with the charge N . For small enough charge, the action becomes negative. The dashed black line is the Giddings-Strominger value of the action.

charge, indicating that such wormholes could break up nonperturbatively into smaller components.

In this theory there also exist solutions with additional oscillations in the fields, a property first observed in [35], see the example in Fig. 27. As one can see there, each oscillation simply adds to the previous solution. That is to say, the solutions with additional oscillations do not display completely different field evolutions, but rather seem to be extensions of solutions with fewer oscillations. As one can also clearly see in the right panel, each oscillation adds a positive contribution to the action, rendering it larger and larger. This implies that oscillating solutions are associated with a lower probability, which is physically reasonable (and differs from the dilatonic case).

In this theory it turns out that the existence of solutions as a function of the axionic charge N is simpler than in the dilatonic case, see Fig. 28. The initial ϕ_0 values lie on monotonic curves. However, the Euclidean action has more notable features, see the right panel in the figure. What jumps out most clearly is that the Euclidean action varies essentially linearly with the charge N , though it is not proportional to it. Also, the action is larger than the GS value at sufficiently large N , but decreases significantly at small N and even reaches negative values, as noticed before in the example of Fig. 24.

The overall structure of the solutions is summarized from a different point of view in Fig. 29, as a function of the charge and the potential width. Solutions exist below the blue line, have action smaller than GS below the green line, and negative action below the red line. Thus, although solutions exist over vast regions of parameter space, it is only in the narrow band between the red and blue lines that

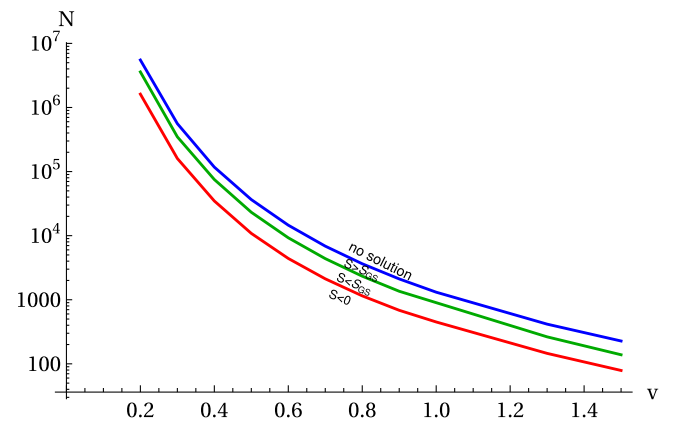


FIG. 29. Existence of expanding wormhole solutions in a double well potential with width v , and for axionic charge N . Results for $v \in [0.2, 1.5]$ have been incorporated. Here $\lambda = 0.01$.

we expect to find physically relevant solutions. Especially in the even narrower band between the red and green lines, we may even expect these solutions to play an important role, as they have higher probabilities associated to them than the corresponding GS wormholes.

V. CONCLUSIONS

We have investigated axion-gravity systems coupled either to a massive dilaton or to a scalar field in a double well potential. In these models we found a whole zoo of wormhole solutions, both generalizations of Giddings-Strominger solutions and what we termed expanding wormholes. The former are characterized by the throat of the wormhole being a local minimum of the geometry, while the latter have a local maximum at the throat and a minimum (or even several minima) further along the geometry. The expanding wormholes thus have a wineglass shape, which implies that after analytic continuation to Lorentzian time, they lead to expanding (rather than contracting) baby universes.

In the scalar field case, we found that the presence of a potential barrier was essential in obtaining wormhole solutions. It is interesting that the existence of a potential barrier was also essential in the recent study, by two of us, of scalar lumps with horizons [36,37], which are solutions that are relevant to gravitational tunneling phenomena, in particular black hole seeded vacuum decay [38,39]. It would be important to see if suitable potential barriers can be obtained in string theoretic models. And, as for the scalar lumps, it would be worthwhile extending the wormhole solutions presented here to different asymptotics, in particular to quasi-de Sitter asymptotics.

The physical meaning of these classical wormhole solutions lies in the role they play in quantum gravity, namely as saddle points of functional integrals. It is clear that in order for a classical solution to be valid, its associated saddle point must have a large action, $S_E \gg \hbar$. In the scalar field case, we found solutions with large action, but we also saw that the action can become small and even turn negative. Here, we may speculate that once the Euclidean action turns negative, the solution may no longer represent a relevant saddle point. This issue will however depend on the contours of integration of the gravitational path integral [40]. It is a general property that a saddle point can only approximate a path integral if its weighting is smaller than the weighting of the geometries that are included in the definition of the integral. Hence, if the gravitational path integral is defined as summing over Lorentzian (pseudo-Riemannian) manifolds, which all have zero Euclidean action, then wormholes with negative Euclidean action (and thus larger weighting than Lorentzian geometries) will simply play no role [41,42]. However, we should point out that the definition of gravitational path integrals is still very much under debate (for recent discussions see [43–45]).

Experience with metastable vacuum decay shows that there are three types of Euclidean solutions with finite action: instantons [46], bounces [47] and oscillating bounces [31]. Instantons interpolate between vacua in a symmetric double well potential, have at most zero modes and describe the mixing of these vacua. Proper bounces in an asymmetric double well have a single negative mode in their spectrum of linear perturbations [48,49], and they describe metastable vacuum decay [50]. Oscillating bounces interpolate between vacua several times, have multiple negative modes [51,52] and their role in vacuum decay remains somewhat obscure. The important question is to which class Euclidean wormholes belong and how we should interpret them. There are several claims in the literature: it was shown in [53] (see also [54,55]) that the GS wormhole has a single negative mode in the lowest (homogeneous) sector. This statement was disproved in [18], where it was shown that with the proper choice of variables there are no homogeneous negative modes about GS wormholes. Later it was claimed that axionic Euclidean wormholes have multiple negative modes with higher angular harmonics [13]. And recently this claim was disputed [14] and it was demonstrated that GS wormholes do not have negative modes at all. We should point out that all of these studies concerned GS wormholes, and that the stability analyses so far included only the axion-gravity system and its fluctuations, without extra fields.

To make progress, it will be important to incorporate the additional scalar or dilaton field. Our findings suggest that the stability analysis will be more involved in those cases. In particular, in the massive dilaton theory we found several different classes of solutions: there are the wormholes continuously connected to GS wormholes for small m^2N and solutions with a “mass gap” which exist only above some minimal m^2N value (and which also exist at large dilaton couplings $\beta > \beta_c$). The latter arise at a bifurcation point. We also found expanding wormhole solutions, which are disconnected from GS wormholes, and also feature bifurcation points. Typically at such bifurcating points the stability properties of solutions change—one branch usually picks up an additional negative mode [56]. Let us recall here that negative modes signal that the solution under consideration is not a true minimum of the action, and that the action can be lowered (and the solution made more relevant) by deforming it in the direction indicated by the negative mode. The puzzling aspect in our case is that we find that typically solutions that have a more complicated field evolution actually have a smaller Euclidean action. The other way around would have appeared more plausible, with negative modes being associated with the extra features. Here, at least naively, it appears that there should be extra negative modes associated with the simpler field evolutions which, if true, would mark a surprising contrast with the purely axionic case. Clearly, an explicit linear stability analysis will be necessary to clarify this question.

This will hopefully also elucidate the meaning of the multi-oscillation wormholes we have found. What might be helpful in addition would be to connect the stability analysis with catastrophe theory, which is a natural mathematical framework for describing such bifurcating behavior.

We leave these intriguing questions for future investigation.

ACKNOWLEDGMENTS

C. J. and J.-L. L. gratefully acknowledge the support of the European Research Council in the form of the ERC Consolidator Grant CoG 772295 ‘‘Qosmology.’’ The work of G. L. is supported in part by the Shota Rustaveli National Science Foundation of Georgia with Grant N FR-21-860 and by the ‘‘EU fellowships for Georgian researchers’’ mobility program.

APPENDIX A: EMBEDDING DIAGRAMS

In order to visualise wormholes it is convenient to use embedding diagrams [57]. Choosing the $h = 1$ gauge in our ansatz (3), and fixing two angular variables on a unit sphere $d\Omega$ properly, we obtain a two dimensional space described by the wormhole metric:

$$ds^2 = d\tau^2 + a(\tau)^2 d\chi^2, \quad (\text{A1})$$

where $\chi \in [0, 2\pi]$ is the angular variable remaining. We want to embed this two dimensional surface in a three dimensional flat Euclidean space with cylindrical coordinates $\{Z, R, \chi\}$:

$$ds^2 = dZ^2 + dR^2 + R^2 d\chi^2, \quad (\text{A2})$$

If the embedded surface is described parametrically by $\{R(\tau), Z(\tau)\}$, then the metric (A2) takes the form:

$$ds^2 = (\dot{Z}^2 + \dot{R}^2) d\tau^2 + R^2(\tau) d\chi^2. \quad (\text{A3})$$

Comparing (A3) with the wormhole metric (A1), we conclude that

$$\dot{Z}^2 + \dot{R}^2 = 1, \quad R(\tau) = a(\tau). \quad (\text{A4})$$

Thus we can express Z as

$$Z(\tau) = \int_0^\tau d\tilde{\tau} \sqrt{1 - \dot{a}^2(\tilde{\tau})}. \quad (\text{A5})$$

Then a revolution plot $\{a(\tau), Z(\tau)\}$ gives the wormhole visualization as shown in Fig. 2.

APPENDIX B: SCALING OF PARAMETERS

Let us count how many free parameters we have.

- (1) Massive dilaton: we may specify the wormhole charge to coupling ratio q/f (or N), the dilaton mass m and the dilatonic coupling constant β .
- (2) Scalar field with double well potential: the action is specified by the wormhole charge to coupling ratio q/f (or N) and the two potential parameters λ and v .

Under the following rescaling of the fields

$$\phi \rightarrow \frac{\phi}{\sqrt{\kappa}}, \quad a \rightarrow \frac{a}{\mu}, \quad h \rightarrow \frac{h}{\mu} \quad (\text{B1})$$

and of the coupling constants to dimensionless variables

$$q \rightarrow \frac{q}{\mu^2 \sqrt{\kappa}}, \quad m \rightarrow \mu m, \quad v \rightarrow \frac{v}{\sqrt{\kappa}}, \quad \lambda \rightarrow \mu^2 \kappa \lambda, \quad (\text{B2})$$

the dependence on μ and κ is removed from the equations of motion and the action scales as

$$S \rightarrow \frac{1}{\kappa \mu^2} S = \frac{1}{\mu^2 / M_{\text{Pl}}^2} S, \quad (\text{B3})$$

where μ is an arbitrary mass scale. In practice, while searching for solutions this scaling freedom allows us to fix one parameter (e.g., m or N in the first theory and λ or N in the second theory) and vary the rest.

APPENDIX C: NUMERICAL ESTIMATION OF WORMHOLE ACTION

For numerical calculations we can divide the wormhole action into two pieces

$$\begin{aligned} S_E &= 2\pi^2 \int_0^{\tau_*} d\tau \left(\frac{2N^2 e^{-\beta\phi\sqrt{\kappa}}}{a^3} - a^3 V \right) \\ &\quad + 2\pi^2 \int_{\tau_*}^{\infty} d\tau \left(\frac{2N^2 e^{-\beta\phi\sqrt{\kappa}}}{a^3} - a^3 V \right) \\ &\equiv S_E^{\text{num}} + S_E^{\text{corr}}, \end{aligned} \quad (\text{C1})$$

where the first part is calculated numerically from $\tau = 0$ to some big $\tau = \tau_*$ and the second part can be analytically estimated as follows. Since we are interested in asymptotically flat solutions, $a(\tau) \rightarrow \tau$ as $\tau \rightarrow \infty$, the scalar field should go asymptotically to its ‘‘vacuum’’ value: $\phi = -v$ in the scalar field case and $\phi = 0$ in the dilaton case. In this setup the leading behavior of the solution of the scalar equation Eq. (7) can be obtained analytically and has the form:

$$\phi(\tau) = \frac{\beta N^2 \sqrt{\kappa}}{M^2 \tau^6} + C_1 \frac{e^{-M\tau}}{\tau^{3/2}} + C_2 \frac{e^{+M\tau}}{\tau^{3/2}} + \dots, \quad (\text{C2})$$

where the dots denote corrections of higher order in $1/\tau$, while M is $\sqrt{2\lambda}v$ in the case of the scalar field and is m in the case of the massive dilaton. It is clear that for a regular solution the last, exponentially growing term should be absent. This can be achieved by adjusting the initial value of the scalar field, while $C_2 \propto (\bar{\phi}_0 - \phi_0)$, where $\bar{\phi}_0$ is the initial value of the scalar field of the

actual regular solution. Using this fact we can estimate S_E^{corr} as

$$S_E^{\text{corr}} = \frac{2\pi^2 N^2}{\tau_*^2} + \dots, \quad (\text{C3})$$

where the dots now denote corrections that are exponentially small and proportional to β/τ_*^8 .

-
- [1] J. A. Wheeler, On the nature of quantum geometrodynamics, *Ann. Phys. (N.Y.)* **2**, 604 (1957).
- [2] S. Carlip, Spacetime foam: A review, *Rep. Prog. Phys.* **86**, 066001 (2023).
- [3] S. B. Giddings and A. Strominger, Axion-induced topology change in quantum gravity and string theory, *Nucl. Phys.* **B306**, 890 (1988).
- [4] S. Hawking, Quantum coherence down the wormhole, *Phys. Lett. B* **195**, 337 (1987).
- [5] G. Lavrelashvili, V. A. Rubakov, and P. G. Tinyakov, Disruption of quantum coherence upon a change in spatial topology in quantum gravity, *JETP Lett.* **46**, 167 (1987).
- [6] G. Lavrelashvili, V. Rubakov, and P. Tinyakov, Particle creation and destruction of quantum coherence by topological change, *Nucl. Phys.* **B299**, 757 (1988).
- [7] S. B. Giddings and A. Strominger, Loss of incoherence and determination of coupling constants in quantum gravity, *Nucl. Phys.* **B307**, 854 (1988).
- [8] S. Coleman, Black holes as red herrings: Topological fluctuations and the loss of quantum coherence, *Nucl. Phys.* **B307**, 867 (1988).
- [9] T. Banks and N. Seiberg, Symmetries and strings in field theory and gravity, *Phys. Rev. D* **83**, 084019 (2011).
- [10] S.-J. Rey, Holographic principle and topology change in string theory, *Classical Quantum Gravity* **16**, L37 (1999).
- [11] J. M. Maldacena and L. Maoz, Wormholes in AdS, *J. High Energy Phys.* **02** (2004) 053.
- [12] N. Arkani-Hamed, J. Orgera, and J. Polchinski, Euclidean wormholes in string theory, *J. High Energy Phys.* **12** (2007) 018.
- [13] T. Hertog, B. Truijen, and T. Van Riet, Euclidean Axion Wormholes have Multiple Negative Modes, *Phys. Rev. Lett.* **123**, 081302 (2019).
- [14] G. J. Loges, G. Shiu, and N. Sudhir, Complex saddles and Euclidean wormholes in the Lorentzian path integral, *J. High Energy Phys.* **08** (2022) 064.
- [15] D. Marolf and H. Maxfield, Transcending the ensemble: Baby universes, spacetime wormholes, and the order and disorder of black hole information, *J. High Energy Phys.* **08** (2020) 044.
- [16] J. McNamara and C. Vafa, Baby universes, holography, and the swampland, [arXiv:2004.06738](https://arxiv.org/abs/2004.06738).
- [17] A. Hebecker, P. Mangat, S. Theisen, and L. T. Witkowski, Can gravitational instantons really constrain axion inflation?, *J. High Energy Phys.* **02** (2017) 097.
- [18] R. Alonso and A. Urbano, Wormholes and masses for Goldstone bosons, *J. High Energy Phys.* **02** (2019) 136.
- [19] P. Betzios, E. Kiritsis, and O. Papadoulaki, Euclidean wormholes and holography, *J. High Energy Phys.* **06** (2019) 042.
- [20] P. Betzios, E. Kiritsis, and O. Papadoulaki, Interacting systems and wormholes, *J. High Energy Phys.* **02** (2022) 126.
- [21] D. Marolf and J. E. Santos, AdS Euclidean wormholes, *Classical Quantum Gravity* **38**, 224002 (2021).
- [22] S. Andriolo, G. Shiu, P. Soler, and T. Van Riet, Axion wormholes with massive dilaton, *Classical Quantum Gravity* **39**, 215014 (2022).
- [23] G. J. Loges, G. Shiu, and T. Van Riet, A 10d construction of Euclidean axion wormholes in flat and AdS space, *J. High Energy Phys.* **06** (2023) 079.
- [24] A. Hebecker, T. Mikhail, and P. Soler, Euclidean wormholes, baby universes, and their impact on particle physics and cosmology, *Front. Astron. Space Sci.* **5**, 35 (2018).
- [25] A. Kundu, Wormholes and holography: An introduction, *Eur. Phys. J. C* **82**, 447 (2022).
- [26] G. Lavrelashvili, V. A. Rubakov, and P. G. Tinyakov, Loss of quantum coherence due to topological changes: A toy model, *Mod. Phys. Lett. A* **03**, 1231 (1988).
- [27] V. A. Rubakov and P. G. Tinyakov, Gravitational instantons and creation of expanding universes, *Phys. Lett. B* **214**, 334 (1988).
- [28] M. Henneaux and C. Teitelboim, p -form electrodynamics, *Found. Phys.* **16**, 593 (1986).
- [29] O. Y. Shvedov, On the exponentially large probability of transition through the Lavrelashvili-Rubakov-Tinyakov wormhole, *Phys. Lett. B* **381**, 45 (1996).
- [30] H. Kim, Axionic wormholes: More on their classical and quantum aspects, *Nucl. Phys.* **B527**, 311 (1998).
- [31] J. C. Hackworth and E. J. Weinberg, Oscillating bounce solutions and vacuum tunneling in de Sitter spacetime, *Phys. Rev. D* **71**, 044014 (2005).
- [32] B.-H. Lee, C. H. Lee, W. Lee, and C. Oh, Instanton solutions mediating tunneling between the degenerate vacua in curved space, *Phys. Rev. D* **82**, 024019 (2010).
- [33] B.-H. Lee, C. H. Lee, W. Lee, and C. Oh, Oscillating instanton solutions in curved space, *Phys. Rev. D* **85**, 024022 (2012).
- [34] G. V. Lavrelashvili, Creation of wormholes during false vacuum decay, *Sov. J. Nucl. Phys.* **45**, 185 (1987).

- [35] G. V. Lavrelashvili, On wormholes in low-energy string theory, *Helv. Phys. Acta* **69**, 245 (1996).
- [36] G. Lavrelashvili, J.-L. Lehners, and M. Schneider, Scalar lumps with a horizon, *Phys. Rev. D* **104**, 044007 (2021).
- [37] G. Lavrelashvili and J.-L. Lehners, Scalar lumps with two horizons, *Phys. Rev. D* **105**, 024051 (2022).
- [38] W. A. Hiscock, Can black holes nucleate vacuum phase transitions?, *Phys. Rev. D* **35**, 1161 (1987).
- [39] R. Gregory, I. G. Moss, and B. Withers, Black holes as bubble nucleation sites, *J. High Energy Phys.* **03** (2014) 081.
- [40] J. Feldbrugge, J.-L. Lehners, and N. Turok, Lorentzian quantum cosmology, *Phys. Rev. D* **95**, 103508 (2017).
- [41] J. Feldbrugge, J.-L. Lehners, and N. Turok, No rescue for the no boundary proposal: Pointers to the future of quantum cosmology, *Phys. Rev. D* **97**, 023509 (2018).
- [42] J. Feldbrugge, J.-L. Lehners, and N. Turok, Inconsistencies of the new no-boundary proposal, *Universe* **4**, 100 (2018).
- [43] J.-L. Lehners, Review of the no-boundary wave function, *Phys. Rep.* **1022**, 1 (2023).
- [44] A. Di Tucci and J.-L. Lehners, No-Boundary Proposal as a Path Integral with Robin Boundary Conditions, *Phys. Rev. Lett.* **122**, 201302 (2019).
- [45] A. Di Tucci, M. P. Heller, and J.-L. Lehners, Lessons for quantum cosmology from anti-de Sitter black holes, *Phys. Rev. D* **102**, 086011 (2020).
- [46] S. R. Coleman, The uses of instantons, *Subnucl. Ser.* **15**, 805 (1979).
- [47] S. R. Coleman, The fate of the false vacuum. 1. Semi-classical theory, *Phys. Rev. D* **15**, 2929 (1977); **16**, 1248(E) (1977).
- [48] A. Khvedelidze, G. V. Lavrelashvili, and T. Tanaka, On cosmological perturbations in closed FRW model with scalar field and false vacuum decay, *Phys. Rev. D* **62**, 083501 (2000).
- [49] M. Koehn, G. Lavrelashvili, and J.-L. Lehners, Towards a solution of the negative mode problem in quantum tunneling with gravity, *Phys. Rev. D* **92**, 023506 (2015).
- [50] S. R. Coleman and F. De Luccia, Gravitational effects on and of vacuum decay, *Phys. Rev. D* **21**, 3305 (1980).
- [51] G. Lavrelashvili, The number of negative modes of the oscillating bounces, *Phys. Rev. D* **73**, 083513 (2006).
- [52] L. Battarra, G. Lavrelashvili, and J.-L. Lehners, Negative modes of oscillating instantons, *Phys. Rev. D* **86**, 124001 (2012).
- [53] V. Rubakov and O. Shvedov, A negative mode about a Euclidean wormhole, *Phys. Lett. B* **383**, 258 (1996).
- [54] J. Y. Kim, H. W. Lee, and Y. S. Myung, Negative modes in the four-dimensional stringy wormholes, *Phys. Rev. D* **56**, 6684 (1997).
- [55] J. Y. Kim, Y.-b. Kim, and J. E. Hetrick, Classical stability of stringy wormholes in flat and AdS spaces, *arXiv:hep-th/0301191*.
- [56] L. Battarra, G. Lavrelashvili, and J.-L. Lehners, Zoology of instanton solutions in flat potential barriers, *Phys. Rev. D* **88**, 104012 (2013).
- [57] C. W. Misner, K. S. Thorne, and J. A. Wheeler, *Gravitation* (W. H. Freeman, San Francisco, 1973).